

## RESEARCH ARTICLE

# The essential *Rhodobacter sphaeroides* CenKR two-component system regulates cell division and envelope biosynthesis

Bryan D. Lakey<sup>1,2</sup>, Kevin S. Myers<sup>1</sup>, François Alberge<sup>1</sup>, Erin L. Mettert<sup>3</sup>, Patricia J. Kiley<sup>3</sup>, Daniel R. Noguera<sup>1,4</sup>, Timothy J. Donohue<sup>1,5\*</sup>

**1** Wisconsin Energy Institute, Great Lakes Bioenergy Research Center, University of Wisconsin-Madison, Madison, Wisconsin, United States of America, **2** Laboratory of Genetics, University of Wisconsin-Madison, Madison, Wisconsin, United States of America, **3** Department of Biomolecular Chemistry, University of Wisconsin-Madison, Madison, Wisconsin, United States of America, **4** Department of Civil and Environmental Engineering, University of Wisconsin-Madison, Madison, Wisconsin, United States of America, **5** Department of Bacteriology, University of Wisconsin-Madison, Madison, Wisconsin, United States of America

\* [tdonohue@bact.wisc.edu](mailto:tdonohue@bact.wisc.edu)



## OPEN ACCESS

**Citation:** Lakey BD, Myers KS, Alberge F, Mettert EL, Kiley PJ, Noguera DR, et al. (2022) The essential *Rhodobacter sphaeroides* CenKR two-component system regulates cell division and envelope biosynthesis. PLoS Genet 18(6): e1010270. <https://doi.org/10.1371/journal.pgen.1010270>

**Editor:** Sean Crosson, Michigan State University, UNITED STATES

**Received:** November 9, 2021

**Accepted:** May 20, 2022

**Published:** June 29, 2022

**Copyright:** © 2022 Lakey et al. This is an open access article distributed under the terms of the [Creative Commons Attribution License](https://creativecommons.org/licenses/by/4.0/), which permits unrestricted use, distribution, and reproduction in any medium, provided the original author and source are credited.

**Data Availability Statement:** All raw and processed ChIP-seq and RNA-seq data are available at NCBI GEO: <https://www.ncbi.nlm.nih.gov/geo/query/acc.cgi?acc=GSE186600>.

**Funding:** This work was supported by the Great Lakes Bioenergy Research Center (<https://www.glbrc.org>), U.S. Department of Energy, Office of Science, Office of Biological and Environmental Research (<https://www.energy.gov/science/ber/biological-and-environmental-research>) (award DE-

## Abstract

Bacterial two-component systems (TCSs) often function through the detection of an extracytoplasmic stimulus and the transduction of a signal by a transmembrane sensory histidine kinase. This kinase then initiates a series of reversible phosphorylation modifications to regulate the activity of a cognate, cytoplasmic response regulator as a transcription factor. Several TCSs have been implicated in the regulation of cell cycle dynamics, cell envelope integrity, or cell wall development in *Escherichia coli* and other well-studied Gram-negative model organisms. However, many  $\alpha$ -proteobacteria lack homologs to these regulators, so an understanding of how  $\alpha$ -proteobacteria orchestrate extracytoplasmic events is lacking. In this work we identify an essential TCS, CenKR (**C**ell envelope **K**inase and **R**egulator), in the  $\alpha$ -proteobacterium *Rhodobacter sphaeroides* and show that modulation of its activity results in major morphological changes. Using genetic and biochemical approaches, we dissect the requirements for the phosphotransfer event between CenK and CenR, use this information to manipulate the activity of this TCS *in vivo*, and identify genes that are directly and indirectly controlled by CenKR in *Rb. sphaeroides*. Combining ChIP-seq and RNA-seq, we show that the CenKR TCS plays a direct role in maintenance of the cell envelope, regulates the expression of subunits of the Tol-Pal outer membrane division complex, and indirectly modulates the expression of peptidoglycan biosynthetic genes. CenKR represents the first TCS reported to directly control the expression of Tol-Pal machinery genes in Gram-negative bacteria, and we predict that homologs of this TCS serve a similar function in other closely related organisms. We propose that *Rb. sphaeroides* genes of unknown function that are directly regulated by CenKR play unknown roles in cell envelope biosynthesis, assembly, and/or remodeling in this and other  $\alpha$ -proteobacteria.

SC0018409 to T. J. D.), and by the National Institutes of General Medical Sciences (Grant R01 GM115894 to P.J.K.). RNA sequencing was conducted by the U.S. Department of Energy Joint Genome Institute, a DOE Office of Science User Facility, which is supported by the Office of Science of the U.S. Department of Energy under contract DE-AC02-05CH11231 (<https://jgi.doe.gov/>). Additional funding provided by the National Science Foundation Graduate Research Fellowship Program (Grant No. DGE-1747503 to B.D.L. (<https://www.nsfgrfp.org/>)), National Institute of Health Genetics Predoctoral Training Program award (T32 GM007133 to B.D.L.), and the Foster Wisconsin Idea Fellowship, UW-Madison, Department of Bacteriology (to B.D.L.). The funders had no role in study design, data collection and analysis, decision to publish, or preparation of the manuscript.

**Competing interests:** The authors have declared that no competing interests exist.

## Author summary

The bacterial cell envelope is home to an array of important functions including energy conservation, motility, influx/efflux of nutrients and toxins, modulation of cell morphology and division, cell-cell interaction, and biofilm formation. Consequently, it is a major target of antibiotics and antimicrobial agents that inhibit these essential processes. Key to the recognition of environmental stressors or stimuli are bacterial TCSs, however systems that monitor or directly regulate cell envelope assembly and homeostasis are not widely conserved amongst bacteria. Here, we use *Rhodobacter sphaeroides* as a model to investigate the function of the CenKR TCS in this and other  $\alpha$ -proteobacteria. We show that this essential TCS plays a key role in maintenance of the cell envelope through the regulation of outer membrane integrity and division, cell wall remodeling and homeostasis, and an alternate sigma factor that controls global cellular stress response. We provide evidence that this TCS and its function is widely conserved in  $\alpha$ -proteobacteria and identify genes of unknown function as candidates for the study of cell envelope assembly in this and related bacteria.

## Introduction

The Gram-negative cell envelope serves as a selectively permeable barrier to separate and protect a cell from its external environment. This inter-connected compartment is comprised of an inner membrane (IM), the periplasmic space, a thin layer of peptidoglycan (PG), and an outer membrane (OM) [1]. The IM is a phospholipid bilayer separating the cytoplasm from the periplasmic space. Encircling the periplasm is the OM, composed of an inner leaflet of phospholipids and an outer leaflet of protective, charged lipopolysaccharides (LPS) that acts as a rigid, semi-permeable barrier [2,3]. Closely associated to the OM is the PG cell wall, a load bearing, mesh-like structure composed of repeating disaccharide units that are cross-linked via short peptide side chains [4,5]. Together, the cell envelope is critical for maintaining cell shape, organizing and facilitating cell division, and protecting cells from deleterious environmental threats such as antibiotics, desiccation, and osmotic stress. Given the many essential functions of the cell envelope, a wide range of naturally occurring toxins, host defense systems, and clinically important antibiotics target cell envelope biosynthetic machinery.

To combat these threats, the Gram-negative cell envelope also serves as a major control center for sensing and rapidly responding to environmental stimuli. Fundamental to this activity are two-component systems (TCSs) which rely on regulated, transmitter-receiver protein communication to monitor cell homeostasis and adjust cell structure, physiology, and behavior in response to internal or external cues [6]. Canonical TCS are comprised of a transmembrane histidine kinase (HK) that upon recognizing an envelope- or extracellular-derived signal autophosphorylates a cytoplasmic C-terminal histidine residue [6–8]. The phosphate of the activated HK is then transferred to its cytoplasmic, cognate response regulator (RR), often resulting in conformational changes and activation of an effector domain to elicit a specific cellular response [6–8]. Commonly, RRs are DNA binding proteins that directly control the transcription of target genes [9]. Several TCSs which regulate envelope functions and mitigate a variety of membrane or cell wall perturbations have been described in Gram-negative bacteria such as *Escherichia coli* Cpx [10–12], Rcs [11–13], and BaeSR [14] and *Caulobacter crescentus* ChvGI [15]. However, these characterized TCS are not generally conserved across bacterial phyla and typically control the transcription of genes whose products are envelope proteases, periplasmic chaperones, function in antibiotic catabolism, or produce alternate PG crosslinks

to maintain cell wall integrity [11,16–21]. Moreover, examples of TCSs that directly regulate cell wall metabolism in *Vibrio cholerae* (WigRK [22]) and *Mycobacterium tuberculosis* (MtrAB [23,24]) are specific to each respective bacterial genus and are necessary for the individual pathogenic lifestyles of these bacteria. Therefore, conserved systems that directly regulate the expression of cell envelope biosynthetic genes remain elusive. Previously, Lemmer *et al.* identified a HK (encoded at the *RSP\_1056* locus) in the Gram-negative  $\alpha$ -proteobacterium *Rhodospirillum rubrum* that when disrupted, resulted in cell envelope changes that included alterations in shape, increased phospholipid content, and sensitivity to detergents and  $\beta$ -lactam antibiotics that target the cell envelope and wall [25]. Together, these results suggested that *RSP\_1056* is a *trans*-membrane HK that plays a previously unknown role in cell envelope homeostasis [25].

In this study, we demonstrate the predicted kinase activity of *RSP\_1056* and identify *RSP\_0847* as the essential cognate RR for this TCS. We apply a systems biology approach, combining genome-scale chromatin immunoprecipitation followed by high-throughput sequencing (ChIP-seq) and analysis of strain specific changes in global transcript abundance (RNA-seq) to identify genes whose expression are directly and indirectly impacted *in vivo* by genetically altering TCS activity. From these data, we identify the direct targets of *RSP\_0847* and make predictions for how the altered transcription of these genes lead to the observed phenotypes of strains with changes in activity of this TCS. Based on these data, we propose that the *RSP\_1056*-*RSP\_0847* TCS, renamed CenK-CenR based on homology with a described TCS in *C. crescentus* [26], is henceforth a regulator of cell division, bacterial envelope development and homeostasis, and OM integrity, specifically through the regulation of the Tol complex. Finally, we show that other  $\alpha$ -proteobacteria of agricultural, industrial, and medical relevance, lacking well-studied cell envelope development and stress responses, contain homologs of this TCS.

## Results

### ***RSP\_1056* is a histidine kinase that phosphorylates the response regulator *RSP\_0847***

To determine how disruption of *RSP\_1056* impacts cellular events [25], we sought to identify the predicted phosphorylation target of *RSP\_1056*. To test that *RSP\_1056* is indeed a HK, we expressed the predicted cytoplasmic portion of this putative *trans*-membrane protein in *E. coli*. After purification, this recombinant form of a truncated *RSP\_1056* was incubated with [ $\gamma$ <sup>32</sup>P]-ATP, and a stable autophosphorylated species corresponding to the molecular weight of the truncated *RSP\_1056* protein was observed (Fig 1A, lane 1), confirming the prediction that *RSP\_1056* is a kinase.

Genes encoding TCS pairs are often found in the same transcriptional unit. However, genomic neighborhood analysis did not identify any putative RR genes in the vicinity of the gene encoding the *RSP\_1056* HK. The *Rb. sphaeroides* genome encodes 27 predicted RRs that are unpaired with corresponding HK genes that could be phosphoacceptors of *RSP\_1056*. To identify potential candidate RRs for the *RSP\_1056* kinase, we used a publicly available *in silico* prediction tool (SwissRegulon -TCS [27]) to infer potential HK-RR orphaned pairs based on conserved sequence-specific interactions between protein domains and specific residues that are canonically involved in phosphotransfer by TCS [27–29]. This approach produced three candidate RRs as phosphoacceptors for *RSP\_1056*. One of these, *RSP\_0847*, had a high Bayesian probability (>0.80) as a phosphoaccepting partner for *RSP\_1056*, while two others (*RSP\_1274* and *RSP\_1083*) had probabilities of 0.14 and 0.05 [27], respectively (S1A Fig). Therefore, we hypothesized that *RSP\_1056* and *RSP\_0847* most likely formed a TCS in *Rb. sphaeroides*.



observed in reactions containing RSP\_0847 (Fig 1A, white arrow), with the appearance of radiolabeled RSP\_0847 after one minute of incubation (Fig 1A, lane 2). Such rapid phosphotransfer from a HK to a RR is characteristic of an interaction between members of known TCSs, as HKs exhibit strong kinetic preference for their *in vivo* cognate RR target *in vitro* [26,30–32]. Using this same assay, we found that phosphotransfer was not observed between RSP\_1056 and the other two candidate RRs (RSP\_1083 and RSP\_1274, S1B Fig). Together, the rapid and specific *in vitro* phosphotransfer between RSP\_1056 and RSP\_0847 provides strong support that these two proteins form a TCS in *Rb. sphaeroides*.

### The gene encoding the RR RSP\_0847 is essential in *Rb. sphaeroides*

A query of the NCBI protein database identified the HK CenK (CCNA\_00564) and RR CenR (CCNA\_03859), Cell envelope Kinase and Regulator, in the  $\alpha$ -proteobacterium *C. crescentus* as potential homologs of RSP\_1056 (35% amino acid identity, E-value  $1e-76$ ) and RSP\_0847 (69.5% amino acid identity, E-value  $2e-107$ ), respectively. In *C. crescentus*, both *cenK* and *cenR* are reported to be essential genes encoded at separate genomic loci, with depletion of either protein resulting in severe OM blebbing and cell lysis through unknown mechanisms [26]. Consistent with the previously proposed essential nature of CenKR, genome-scale Tn-seq analysis of *Rb. sphaeroides* (S2A and S2B Fig) predicted that the gene encoding the RR RSP\_0847 was essential [33]. However, unlike in *C. crescentus*, this analysis identified transposon insertions in RSP\_1056 suggesting this gene is not essential in the conditions tested [25,33].

To independently test if RSP\_0847 is an essential gene, we attempted to construct an in-frame deletion of this gene using the same method that we used to generate an in-frame deletion of RSP\_1056 (Fig 1B). We were unable to recover a strain containing a chromosomal deletion of RSP\_0847, confirming its essentiality in *Rb. sphaeroides*. To independently confirm the functionality of the recombineering plasmid, we attempted to recover a chromosomal deletion of RSP\_0847 in a strain constitutively expressing RSP\_0847 from an ectopic plasmid (S2B and S2E Fig). We were able to efficiently recover in-frame deletions of the genomic copy of RSP\_0847 in this background (S2C Fig) confirming the efficacy of our plasmid to inactivate this locus. Together, these biochemical and genetic analyses provide evidence that the *Rb. sphaeroides* RSP\_1056-RSP\_0847 TCS is likely a homolog of *C. crescentus* CenKR [26]. Therefore, we will hereafter refer to RSP\_1056 as *cenK* and RSP\_0847 as *cenR*.

### Aspartate 56 in CenR is critical for phosphorylation by CenK

To further explore the impact and mechanism of phosphotransfer from CenK to CenR, we sought to identify the CenR residue that was required for phosphorylation by CenK. To do this, we used the I-TASSER homology modeling tool [34–36] to predict which CenR aspartate residue acts as a phosphoacceptor from CenK. The receiver domain of OmpR-family RRs, like CenR, contains five-stranded parallel  $\beta$ -sheets flanked by two  $\alpha$ -helices on the N-terminus and three  $\alpha$ -helices on the other, with the canonical phosphoaccepting aspartate residue located at the end of the third  $\beta$ -sheet [7,8]. This residue is located proximal to negatively charged residues between  $\alpha 1$  and  $\beta 1$ , which coordinate a  $Mg^{2+}$  ion to catalyze phosphorylation [7,8]. The I-TASSER structural model of CenR (Fig 1C) we used was assembled based on similarity to the structure of a RR in *M. tuberculosis* (PDB accession number: 1YS6; identity 0.31, coverage 0.97, TM-score 0.87, RMSD 2.16). This model predicts that residue D56 in CenR (Fig 1C, magenta) is proximal to the three aspartate residues, D11-D13, that coordinate  $Mg^{2+}$  (Fig 1C, orange), and likely the residue that participates in phosphotransfer from CenK.

To assess if an aspartate at residue D56 is needed for CenR phosphorylation, we expressed and purified a variant RSP\_0847 protein containing an alanine substitution (D56A) and tested for activity in a phosphotransfer assay with  $^{32}\text{P}$ -labeled CenK (Fig 1D). We observed no transfer between  $^{32}\text{P}$ -labeled CenK and CenR(D56A) under the same conditions where wild-type RR was phosphorylated, demonstrating that an aspartate at residue 56 is necessary for this protein to serve as a phosphoacceptor from phosphorylated CenK. Previously, it had been proposed that *Rb. sphaeroides* CenR residue D51 is a site of phosphorylation [37]. However, given the predicted orientation of the CenR D51 side chain away from the catalytic phosphorylation site at the N-terminus of  $\beta 1$ , and the inability of CenR(D56A) to be phosphorylated by CenK *in vitro*, we propose that D56 is the site of phosphorylation of this RR (Fig 1C).

### Modulation of the activity of CenR results in cell length defects

Using this *cenR*(D56A) allele, we asked if we could disrupt phosphorylation of CenR *in vivo*. As we were able to delete *cenK* (Fig 1B), we hypothesized that a non-phosphorylatable form of CenR would be sufficient to support cell viability and would phenocopy cells containing the  $\Delta cenK$  allele. To test this hypothesis, we successfully created a strain containing an alanine codon at residue D56 of the native *cenR* locus (*cenR*(D56A)), using the same methods that were unable to produce a strain containing an in-frame deletion of *cenR*.

As previous studies showed that loss of CenK had an observable impact on cell shape [25], we tested the impact of the CenR D56A substitution *in vivo* by measuring cell dimensions using bright-field microscopy. We observed that cells containing the *cenR*(D56A) allele were short (length: WT =  $1.98 \pm 0.11 \mu\text{m}$ ; *cenR*(D56A) =  $1.63 \pm 0.10 \mu\text{m}$ ;  $\Delta cenK$  =  $1.62 \pm 0.13 \mu\text{m}$ ) and more spherical (width: WT =  $0.66 \pm 0.04 \mu\text{m}$ ; *cenR*(D56A) =  $0.80 \pm 0.04 \mu\text{m}$ ;  $\Delta cenK$  =  $0.82 \pm 0.05 \mu\text{m}$ ) in comparison to wild-type cells (Fig 2A–2C). As the *cenR*(D56A) allele phenocopied the features of the  $\Delta cenK$  strain, this supports the conclusion that reduction in activity of this TCS is the cause of the observed changes in cell shape. Furthermore, *Rb. sphaeroides* cells containing either the  $\Delta cenK$  or *cenR*(D56A) alleles grew at a similar rate compared to wild-type cells (doubling time:  $\sim 2.5$  hrs) and reached a similar final cell density (Fig 2D). From our *in vitro* and *in vivo* data, we conclude that the CenR D56A amino acid substitution reduces but does not completely abolish activity of the CenKR TCS.

It has been established that substitution of the phosphoaccepting aspartate residue with a glutamate can sterically mimic phosphorylation of other RRs [38,39]. Therefore, we hypothesized that introduction of the phosphomimetic amino acid change D56E in CenR would result in a cell elongation phenotype. We generated a strain containing a glutamate codon at position 56 of the native *cenR* locus (*cenR*(D56E)), and measured cell dimensions finding that *cenR*(D56E) cells were longer ( $2.91 \pm 0.17 \mu\text{m}$ ) than wild-type cells (Fig 2A and 2C). We also observed that cells containing the *cenR*(D56E) allele grew slower than wild-type cells (*cenR*(D56E)  $\sim 3.5$  hrs, WT  $\sim 2.5$  hrs, Fig 2D) suggesting that constitutive activity of CenR has pleiotropic effects on growth and/or cell division rates. To test if the impact of the *cenR*(D56E) allele is independent of CenK activity, we introduced this mutation in a  $\Delta cenK$  strain. We observed  $\Delta cenK$  *cenR*(D56E) also produced longer cells than those containing a wild-type CenR protein (S3 Fig,  $2.91 \pm 0.06 \mu\text{m}$ ), confirming that the D56E substitution in CenR is sufficient to increase the activity of the RR and change cell length and growth rate.

### Characterization of the genome-wide binding sites of CenR

To understand how changes in CenKR activity led to the observed cellular changes, we sought to identify genes comprising the direct regulon for this TCS (Fig 3). We expected CenR to bind DNA since it is predicted to be within the OmpR RR family and contains a characteristic

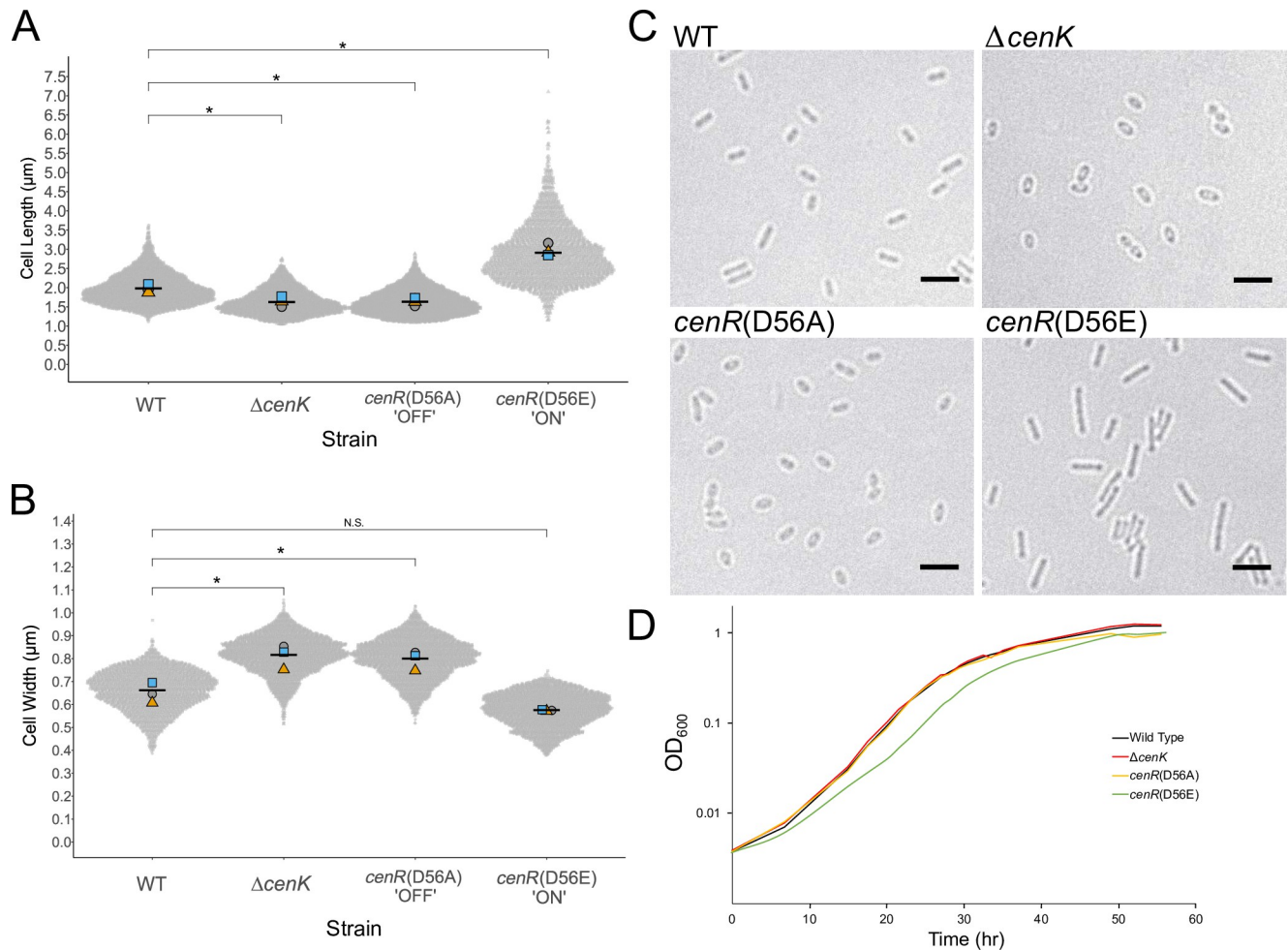


**Fig 2. Impact of changes in CenKR activity on cell dimensions.** (Panels A-C) Bright-field microscopy measurements of the length and width of exponential phase cells displayed as beeswarp plots [135]. Mean values from each of the three biological replicates (grey circles, yellow triangles, and blue squares, respectively) and mean values for each strain are shown (black bar). For each biological replicate, >1000 cells were analyzed. Unpaired t-tests were used to compare pooled cell dimension data from the mean values of each biological replicates ( $n = 3$ ) [133]. Significant  $P$  values < 0.05 are indicated by an asterisk. (A) Cell length measurements of wild-type (WT) and indicated CenKR mutants: (mean  $\pm$  SD) WT =  $1.98 \pm 0.11 \mu\text{m}$ ;  $\Delta cenK$  =  $1.62 \pm 0.13 \mu\text{m}$ ; *cenR(D56A)* =  $1.63 \pm 0.10 \mu\text{m}$ ; *cenR(D56E)* =  $2.91 \pm 0.17 \mu\text{m}$  (see text for explanation of individual alleles). (B) Cell width measurements of WT and indicated CenKR mutants: WT =  $0.66 \pm 0.04 \mu\text{m}$ ;  $\Delta cenK$  =  $0.82 \pm 0.05 \mu\text{m}$ ; *cenR(D56A)* =  $0.80 \pm 0.04 \mu\text{m}$ ; *cenR(D56E)* =  $0.57 \pm 0.01 \mu\text{m}$ . (C) Bright-field microscopy images of wild-type and indicated CenKR mutant strains (scale bar = 3  $\mu\text{m}$ ). (D) Growth curve of *Rb. sphaeroides* strains. Hyperactivation of CenR results in slower growth rate compared to WT cells (3.5 hours vs 2.5 hour doubling time, respectively).

<https://doi.org/10.1371/journal.pgen.1010270.g002>

winged helix-turn-helix motif in the C-terminal effector domain of the protein (Fig 1C) [6]. To identify potential CenR binding sites, we used ChIP-seq to map the *in vivo* DNA binding by this protein in strains containing wild-type, increased (*cenR(D56E)*), and decreased ( $\Delta cenK$  or *cenR(D56A)*) activity of this TCS. Using the MOSAiCS [40] peak finding algorithm, we identified 458 sites across the *Rb. sphaeroides* genome as putative CenR binding sites (S1 Data). Of these, ~60% (273) were present in three or more biological replicates and were located near previously mapped transcription start sites (TSSs) of cells grown under the same conditions used to monitor DNA binding by this RR [41]. The remaining ~40%, found in less than three biological replicates, located in intragenic regions, or between coding regions of convergent genes, were not used in the subsequent analysis.

To identify the CenR binding events which led to changes in gene expression, we used RNA-seq to compare global transcript levels in the same strains used for ChIP-seq experiments

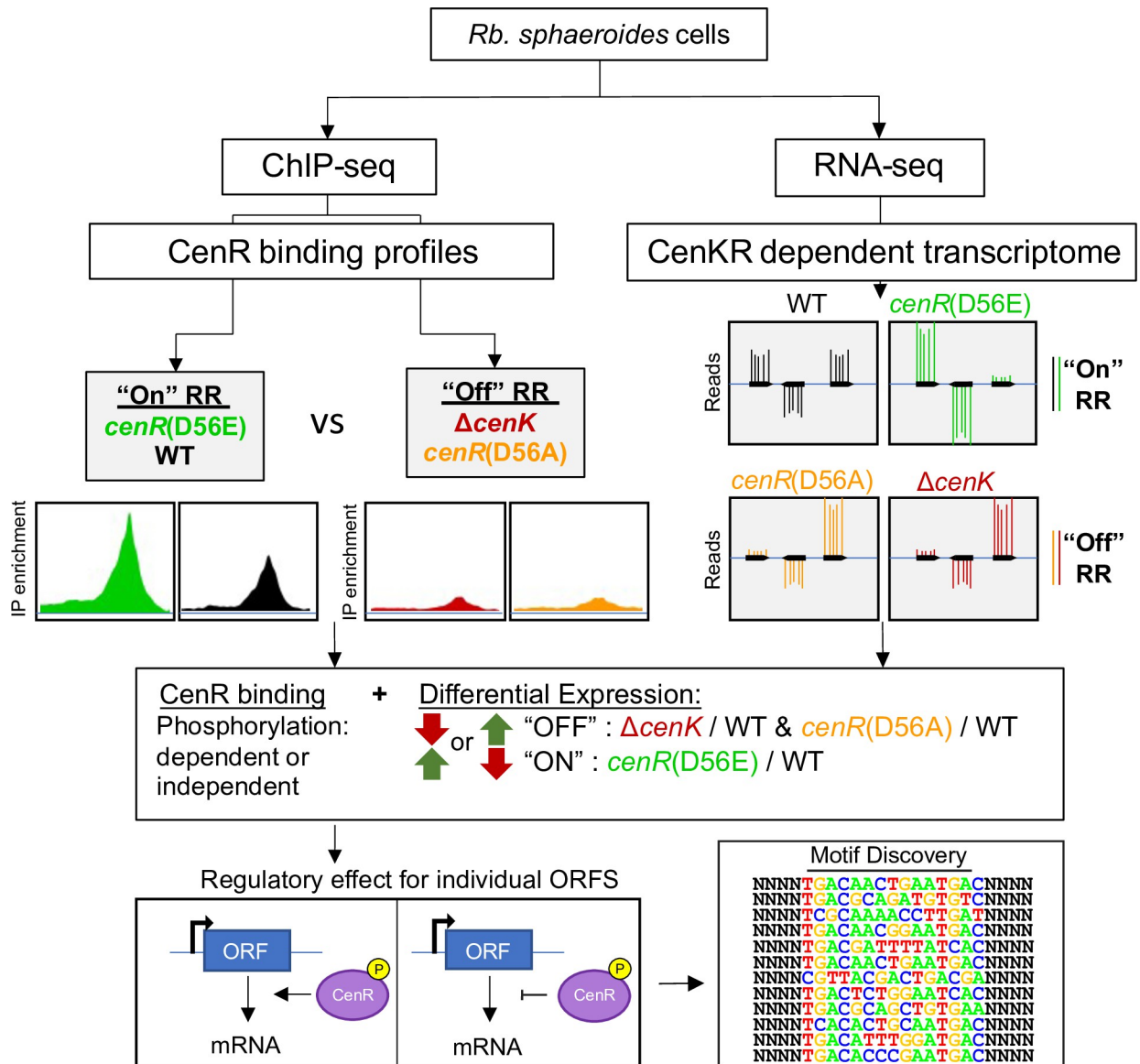


**Fig 3. Strategy used to define members of the CenKR regulon.** The *in vivo* genome-wide CenR binding sites and CenKR-dependent transcriptomic data were generated from strains with a hyperactive (CenR D56E), wild-type (WT), and low activity (CenR D56A and  $\Delta$ CenK) TCS. Combined data sets were used to identify genes directly regulated by CenR and the mode of regulation of each candidate gene. Genomic CenR binding sites were then analyzed for a putative DNA binding motif recognized by CenR to further refine the predicted CenR regulon.

<https://doi.org/10.1371/journal.pgen.1010270.g003>

(S2 Data). A total of 597 genes were differentially expressed in at least two strains with  $\log_2$ -fold change greater than 0.5 or less than -0.5 and a false discovery rate (FDR) of less than 0.05. Based on the impact of CenR amino acid changes at residue D56 on cells, we predicted that genes with increased transcript levels in a strain containing a hyperactive TCS (CenR D56E) should show decreased expression in cells containing reduced CenKR activity (CenR D56A), and vice versa. Of the 597 differentially expressed genes (DEGs) among these data sets, 275 showed opposing expression patterns when comparing strains with increased and decreased CenKR activity relative to wild-type (S2 Data). Combining the ChIP-seq results mapping CenR binding sites and transcriptomic analysis of CenKR dependent changes in gene expression, we identified 59 potential transcriptional units (101 DEGs) that both showed CenR DNA binding

and differential transcripts levels between wild-type cells and TCS mutants (S1 Table). Of the 59 potential transcriptional units identified, we predict that CenR activates the expression of 42 (71%), while repressing transcription of the other 17 (29%).

### Identification of a CenR binding motif

We used MEME [42,43] to identify a conserved DNA sequence logo enriched in regions defined by the 59 ChIP-seq peaks mentioned above. This analysis identified the motif sequence TGA-N<sub>8</sub>-TGA (Fig 4A), a tandem direct repeat within <100 bp upstream of 31 of these 59 putative CenR regulated transcriptional units (S1 Table). Identification of a direct repeat is consistent with other OmpR family transcription factors that often bind DNA as oligomers by recognizing direct repeat sequence motifs [9]. Additionally, the 10 bp distance between the start of each half-site is consistent with that of other known RR that bind B-form DNA [9,44].

We compared the position of each identified CenR binding site to the TSS of each transcriptional unit to make predictions on the role of this RR in controlling expression of these genes (Fig 4C and 4D). Based on this analysis, we found that 28 of the 31 CenR binding sites are located directly upstream of the promoter -35 element (Fig 4C and 4D, green) and oriented co-directionally with the direction of transcription. The location of these predicted CenR binding sites relative to the promoter of these transcription units is consistent with our hypothesis that this RR activates transcription of these genes, likely through interacts with the  $\alpha$  subunit of RNA polymerase analogous to other OmpR-family RRs [9]. Of the transcriptional units that we predicted are directly repressed by CenR, the predicted RR binding site is located between the -35 promoter element and known TSS (Fig 4C and 4D, red), with two of the predicted binding sites oriented in the opposite direction of transcription, and one co-directional. This suggests that CenR binding to these sites represses transcription by competing for RNA polymerase binding to promoter elements. Together, we propose that the 31 transcriptional units that contain the conserved TGA-N<sub>8</sub>-TGA motif are members of the CenKR direct regulon (Table 1). While we were unable to find this putative CenR binding site upstream of the other 28 transcriptional units, this does not necessarily mean that these transcriptional units are not direct members of this regulon. However, for this study, we only considered transcriptional units with CenR binding sites in the subsequent analyses.

To test the role of the TGA-N<sub>8</sub>-TGA direct repeat in CenR binding to promoter regions, we assayed the ability of phosphorylated CenR (CenR~P) to bind to DNA fragments containing the promoter regions of *rpoH1* and *tolQRAB* which are predicted to contain a related sequence (Table 1) and *RSP\_2157* which lacks any similarity to this motif. When we assayed binding of CenR~P to each DNA fragment in a gel electromobility shift assay (EMSA), we found that the presence of CenR~P in reactions containing DNA fragments of either *rpoH1* or *tolQRAB* transcriptional units resulted in delayed migration through the gel, relative to reactions containing no protein, which is indicative of DNA-protein interaction (S5 Fig). Furthermore, we observed no change in migration patterns of the DNA fragment of the *RSP\_2157* promoter suggesting that the shift in *rpoH1* or *tolQRAB* promoter DNA was dependent on the presence of the TGA-N<sub>8</sub>-TGA direct repeat sequence. The binding patterns observed in this EMSA were similar to what has been previously reported for other OmpR family response regulators, like ArcA, which recognizes a series of three direct repeat motifs [47,48]. Together, this bioinformation and *in vitro* data suggest that this direct repeat is likely the DNA binding motif recognized by CenR *in vivo*.

### CenKR directly activates the expression of genes for envelope stress, remodeling, and cell division

We used the known or predicted function of the DEGs to gain insight into cellular functions that are directly controlled by CenR. Of the 31 transcriptional units which we predict are direct

**Table 1. The CenKR regulon.**

CENTER OF PEAK (bp) <sup>a</sup>	CHIP-seq FOLD ENRICHMENT (IP/INPUT)		DOWNSTREAM GENE		TM Domains <sup>b</sup>	Signal Peptide <sup>c</sup>	Predicted DNA-binding motif: TCA-N8-TCA	TRANSCRIPT FOLD CHANGE (log <sub>2</sub> ) <sup>d</sup>						REGULATORY ROLE <sup>e</sup>	Essential <sup>f</sup>			
	D56E	WT	ΔcenK	D56A				GENE NAME	ANNOTATION	cenR (D56E)	FDR	ΔcenK	FDR			cenR (D56A)	FDR	
<b>Cell envelope, transport, and extracytoplasmic targeted proteins</b>																		
2597500	1.4	--	--	--	RSP_0847	RSP_0847	two component transcriptional regulator winged helix family	N	N	ACACGAGCGGTGAG	0.49	9.1E-07	-5.16	5.9E-07	-4.34	1.1E-06	+	Y
2413901	4.5	3.2	1.6	1.6	RSP_0672	tolQ	Cell division and transport-associated protein TolQ	Y	N	TGACCGCAGATGTT	2.51	2.3E-03	-0.58	6.7E-03	n.s.	n.s.	+	Y
392575	3.8	1.7	--	--	RSP_1807	RSP_1807	putative secreted protein	N	Y	TCGCAAAAACCTTGAT	2.72	4.1E-06	-2.04	1.4E-04	-1.97	8.0E-05	+	N
426084	2.8	2.3	--	--	RSP_1834	RSP_1834	Beta-lactamase superfamily	N	Y	TGACCGCAGCTGAA	2.47	4.4E-06	-5.56	1.7E-05	-5.43	2.8E-07	+	N
2970115	2.9	2.2	--	--	RSP_1199	RSP_1199	L,D-transpeptidases/carboxypeptidases	N	Y	TGACGGCGGGTGA	2.47	4.4E-05	-1.98	9.9E-05	-1.39	5.1E-04	+	N
2970115*	2.9*	2.2*	--	--	RSP_1200	RSP_1200	uncharacterized protein with SCP/PR1 domains	Y	Y	TGACATGGCAATTGAA	0.52	1.6E-05	-0.52	3.7E-03	n.s.	n.s.	+	N
478200	2.0	1.6	--	--	RSP_1880	RSP_1880	peptidoglycan-binding domain-containing protein	N	Y	TCACATGGCCGTGTT	-1.80	4.6E-06	1.24	5.3E-03	n.s.	n.s.	-	N
2933000	1.8	1.4	--	--	RSP_1168	surA	PpIC-type peptidyl-prolyl cis-trans isomerase	N	Y	TGACATGATCGTGTG	3.40	2.8E-06	-1.48	9.1E-04	-0.74	1.1E-02	+	N
2933000*	1.8*	1.4*	--	--	RSP_1169	secA	protein translocase subunit secA	N	N	TCGCGCGACGTTGAC	1.80	3.0E-06	-0.94	1.7E-03	n.s.	n.s.	+	Y
435330	2.0	--	--	--	RSP_1844	RSP_1844	putative periplasmic protein	N	Y	TGGCGCAGGGTGC	1.25	2.2E-05	n.s.	n.s.	n.s.	n.s.	+	N
1368770	2.0	--	--	--	RSP_2718	RSP_2718	putative outer membrane protein	Y	Y	TCACCTCCTCGTGC	3.09	8.2E-04	-4.76	5.9E-07	-6.49	2.9E-07	+	N
2641460	1.8	--	--	--	RSP_0890	mhaC	Intermembrane phospholipid transport system binding protein	N	Y	TCATACTTGGTGAT	2.47	1.7E-03	-0.74	2.2E-03	-1.14	6.9E-04	+	N
2473818	3.2	1.9	--	--	RSP_0730	RSP_0730	TIGR02302 family protein	Y	N	TCACTTCGCGTTCAT	2.23	2.0E-04	-1.63	3.7E-04	-0.63	1.5E-02	+	N
2450500	2.0	1.4	--	--	RSP_0704	RSP_0704	ABC peptide transporter substrate binding protein	Y	Y	TCACGCAATCGCAAC	1.77	2.1E-05	-0.62	4.0E-03	n.s.	n.s.	+	N
458700	1.6	1.7	--	--	RSP_1860	RSP_1860	cell wall hydrolase involved in spore germination	N	Y	TGGCAAAAATGTCAC	1.42	2.1E-03	-0.61	1.1E-02	-1.25	6.6E-04	+	N
1458970	1.6	1.6	--	1.6	RSP_2847	RSP_2847	putative lipoprotein (predicted lipid binding domain)	Y	Y	TCTTCGTCCCTGC	-1.20	1.1E-03	0.97	2.7E-02	n.s.	n.s.	-	N
2665900	1.5	--	--	--	RSP_0915	RSP_0915	putative periplasmic protein	N	Y	TGACAAAACGTTAG	1.43	5.7E-04	n.s.	n.s.	n.s.	n.s.	+	N
606400	1.6	--	--	--	RSP_2006	RSP_2006	uncharacterized protein involved in outer membrane biogenesis	Y	N	TCACGCAATCCTGC	0.67	7.9E-04	n.s.	n.s.	n.s.	n.s.	+	N
930800 (chr2)	1.7	1.6	--	--	RSP_1413	RSP_1413	TRAP-T family transporter periplasmic binding component	Y	Y	TCACAAATGCATTAC	-1.34	1.2E-02	0.89	5.8E-02	n.s.	n.s.	-	N
1207306	2.7	1.8	--	1.5	RSP_2561	expP	putative succinoglycan biosynthesis transport protein ExpP	Y	N	TCACGATCCTCAG	n.s.	n.s.	n.s.	n.s.	-0.60	4.2E-02	+	N
278100	1.7	--	--	--	RSP_1024	RSP_1024	Putative MoxR family protein	Y	N	TCACGATCAATTTGTG	0.85	9.1E-05	-0.56	6.1E-03	-0.84	3.8E-03	+	N
2758300	2.8	1.5	--	--	RSP_1000	dsbC	Disulphide bond corrector protein DsbC	N	Y	TGGCGCAGTTGTGC	2.48	5.9E-06	-1.64	1.9E-03	-2.07	8.8E-05	+	N
2758300*	2.8*	1.5*	--	--	RSP_0999	RSP_0999	putative transcriptional regulator	N	N	TCGCGCGACTGTGGC	1.37	4.5E-05	n.s.	n.s.	n.s.	n.s.	+	N
1273100	1.6	--	--	--	RSP_2633	cmfF	Cytochrome c maturation protein CmfF	Y	N	TGACGGGAAAGCGAC	1.06	3.2E-02	-0.21	3.0E-02	n.s.	n.s.	+	Y

(Continued)

Table 1. (Continued)

CENTER OF PEAK (bp) <sup>a</sup>	ChIP-seq FOLD ENRICHMENT (IP/INPUT)		DOWNSTREAM GENE		TM Domains <sup>b</sup>	Signal Peptide <sup>c</sup>	Predicted DNA-binding motif: TGA-N8-TGA	TRANSCRIPT FOLD CHANGE (log <sub>2</sub> ) <sup>d</sup>				REGULATORY ROLE <sup>e</sup>	Essential <sup>f</sup>					
	D56E	WT	ΔcenK	D56A				ID	GENE NAME	ANNOTATION	FDR			ΔcenK	FDR	cenR (D56E)	cenR (D56A)	FDR
Cell envelope, transport, and extracytoplasmic targeted proteins																		
1330900	2.2	--	--	--	RSP_2685	<i>cycH</i>	Putative cytochrome c-type biogenesis protein <i>cycH</i>	Y	N	TGACGGGATAATTGAC	0.79	1.1E-04	n.s.	n.s.	-0.89	1.6E-02	+	Y
1330900*	2.2*	--	--	--	RSP_2686	<i>soxB</i>	putative sarcosine oxidase beta subunit	N	N	TCGCAACTCGGTGAT	3.76	6.0E-05	-1.21	5.5E-04	n.s.	n.s.	+	N
51549	1.9	1.5	--	--	RSP_1465	<i>RSP_1465</i>	putative aminoglycoside phosphotransferase	N	N	TCACGCAATCTTTAT	0.78	4.5E-05	-1.14	1.2E-03	-1.42	1.6E-03	+	N
106900 (chr2)	1.6	--	--	--	RSP_3067	<i>RSP_3067</i>	hypothetical protein	Y	N	TCGCAGGATCTTGAT	4.51	1.9E-06	n.s.	n.s.	-1.27	8.0E-03	+	N
84880	2.5	1.6	--	--	RSP_1496	<i>RSP_1496</i>	Lysosome-like putative lipoprotein	N	Y	TCGGTTTTCTTGAA	1.37	1.3E-03	n.s.	n.s.	n.s.	n.s.	+	N
Cytoplasmic proteins																		
1059245	4.1	2.5	--	--	RSP_2410	<i>rpoH1</i>	RNA polymerase sigma 32 subunit—RpoH	N	N	TTACATTCGGGTGAT	3.20	3.2E-04	-3.38	1.4E-06	-2.30	4.6E-06	+	N
2296600	1.6	--	--	--	RSP_0559	<i>msrA</i>	Peptide methionine sulfoxide reductase	N	N	TGGCGCGAGCGTGAT	3.11	8.92E-06	-1.78	1.6E-04	-1.41	4.1E-04	+	N

<sup>a</sup>Chromosomal position of ChIP-seq peak (chr2—chromosome 2)

<sup>b</sup>Transmembrane domain predicted using TMHMM 2.0 [45]

<sup>c</sup>Signaling transit peptides identified using SignalP 5.0 [46], scores ≥ 0.6 were interpreted to have predicted transit peptides

<sup>d</sup>log<sub>2</sub>(Fold-Change) are reported relative to WT (i.e. mutant/WT)

<sup>e</sup>Regulatory role of CenR based on changes in gene expression between TCS mutants relative to WT cells. (+) positively regulated by CenR, (-) negatively regulated by CenR, (NA) Not assigned from data

<sup>f</sup>Essentiality determined previously by Tn-seq analysis [33]

-- No significant ChIP enrichment

\* Peak located between differentially expressed genes

n.s. Not significant, RNA FDR p-value > 0.05 cutoff

<https://doi.org/10.1371/journal.pgen.1010270.t001>

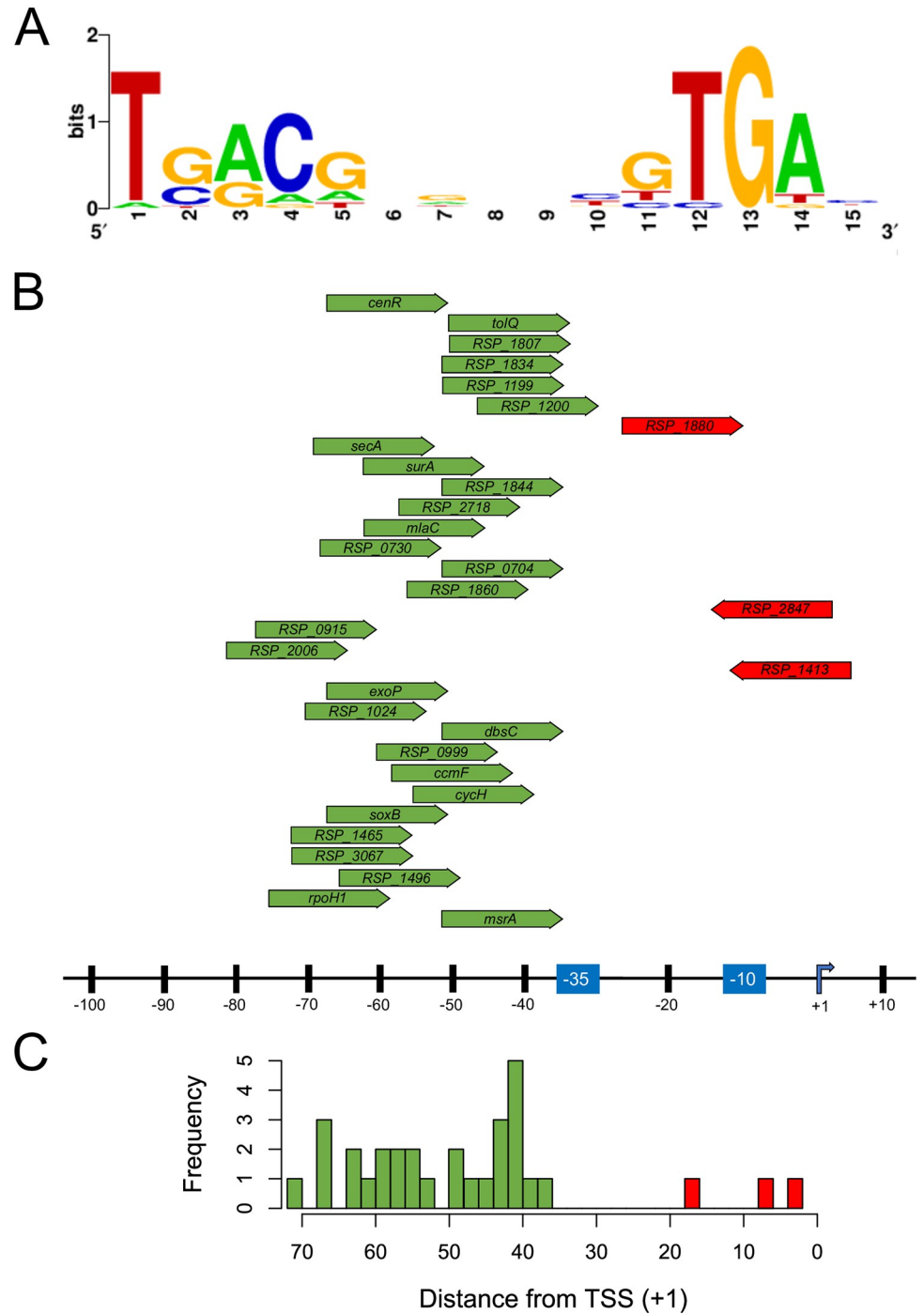


**Fig 4. Identification of the CenR DNA binding motif.** (A) WebLogo [134] representation of CenR consensus sequence determined using the MEME motif finder. Of the 59 promoters identified in ChIP-seq experiments, 31 operons contained the putative CenR consensus sequence TGA-(N8)-TGA. (B) Location and orientation of the 31 identified CenR binding sites, in respect to the previously determined TSS [41] and promoter -35 and -10 elements [126] for directly activated (green) and repressed (red) transcription units. The DNA sequence of each binding motif is listed in Table 1. (C) Histogram of the distance from the center of each putative CenR binding site and the TSS of the respective transcription unit mapped in (B). Operons predicted to be activated have CenR binding sites upstream of the -35 promoter element, whereas operons predicted to be repressed have CenR binding sites that overlap either the TSS or the predicted promoter elements.

<https://doi.org/10.1371/journal.pgen.1010270.g004>

targets for control by CenR, 29 encode protein products that are targeted to the cell envelope or periplasmic space (Table 1), illustrating this TCS plays a broad role in the function of this cellular compartment. For example, we identified CenR as a direct activator of the transcriptional unit that encodes the Tol proteins of the Tol-Pal complex. CenR enrichment was identified upstream of *tolQ*, the first gene in the *tolQRAB* operon, in all strains analyzed, with decreased occupancy of this RR in  $\Delta$ *cenK* and *cenR*(D56A) strains (Fig 5A). We found increased abundance of *tolQRAB* transcripts in cells with increased CenKR activity relative to wild-type cells and a slight, yet significant decrease in abundance of the same transcripts in cells with reduced activity of this TCS (Fig 5A).

We found that the expression of other genes known or predicted to function in cell envelope maintenance in other bacteria were predicted to be directly activated by CenR (Table 1). For example, *RSP\_1834* encodes a predicted  $\beta$ -lactamase that, in other bacteria, degrades antibiotics that target penicillin binding proteins thereby preventing inhibition of PG synthesis [49], and *RSP\_1199* which encodes a putative L,D-transpeptidase that forms crosslinks between peptide sidechains of PG either in response to OM/LPS assembly defects, osmotic stress, or in response to  $\beta$ -lactam antibiotics that inhibit D,D-transpeptidases [5,50,51]. Moreover, *Rb. sphaeroides* genes encoding proteins that function in autolysis to digest glycan chains of PG such as *RSP\_1496* (a putative lysozyme-like lipoprotein), and *RSP\_1860* (a putative cell wall hydrolase) are among those that we predict are directly regulated by CenKR (Table 1). We also identified CenR as a direct transcriptional regulator of the gene encoding the periplasmic retrograde lipid trafficking protein MlaC (*RSP\_0890*), a member of the Mla complex (maintenance of lipid asymmetry) and functions to transport lipids away from the OM [52]. *RSP\_0915*, *RSP\_1200*, *RSP\_1844*, *RSP\_2006*, *RSP\_2718*, and *RSP\_3067* are genes of unknown function that encode proteins targeted to the OM or periplasmic space in other bacteria, suggesting that these predicted members of the direct CenR regulon may have heretofore untested roles in cell envelope biology in *Rb. sphaeroides* and other related  $\alpha$ -proteobacteria.

This analysis also predicted that several of the gene products in the direct CenR regulon aid in the mitigation of misfolded proteins. These include the homolog of the *E. coli* periplasmic chaperon, SurA, which functions to facilitate the folding and assembly of OM proteins [53], and the alternate sigma factor RpoHI (Fig 5B). *Rb. sphaeroides* RpoHI directly controls genes encoding protein that are involved in protein homeostasis, maintenance of membrane integrity, and DNA repair [54], and we identified many of these genes as DEGs in our RNA-seq datasets (S2 Data). This latter result suggests that CenKR initiates a global response to general stress. Furthermore, we predict that CenR directly regulates genes that mitigate oxidative and disulfide bond protein stresses *dsbC*, *msrA* [55,56], and cytochrome biogenesis operons *ccmF-ccmH* as well as *cycH*. Finally, RRs often regulate their own transcription [9,29]. Consistent with this, we observed CenR binding upstream of *cenR* (Fig 5C), but not upstream of *cenK*. Accordingly, we observed no change in transcription of *cenK*, suggesting expression of *cenK* is not dependent on CenKR activity (Fig 5C).

### Cell wall biosynthetic machinery indirectly responds to changes in CenKR activity

Transcripts from genes encoding PG biosynthesis machinery critical for division and elongation were differentially expressed in cells with altered CenKR activity (Fig 5D). Cells containing the *cenR*(D56E) allele had reduced levels of transcripts from genes whose products are predicted to function in synthesis of cytoplasmic PG precursor molecules (*murB*, *murC*, *murD*, *murE*, *ddlA*, *murF*, *mraY*, and *murG*), their transport across the inner membrane (*ftsW*), and their subsequent assembly into nascent peptide chains (*ftsA*, *ftsQLB*, *ftsK*



(*RSP\_1495*), *ftsX* (*RSP\_0734*), *ftsN* (*RSP\_6008*), *pbp1B* (*RSP\_0887*), *pbp1C* (*RSP\_1355*) [5,57]. We also found an effect of the *cenR*(D56E) allele on the abundance of transcripts from genes whose products are predicted to function in the divisome (Fig 5D), the complex involved in septal PG synthesis during the latter stages of cell division [5,57]. We found that cells containing the *cenR*(D56E) allele had increased levels of transcripts from genes predicted to encode subunits of the Rod complex (Fig 5D) that synthesizes PG along the lateral cell wall to facilitate cell elongation [5,57]. Combined, these changes in transcript abundance provide a possible explanation for the cell length changes observed in cells that contain the *cenR*(D56E) allele which we predicted increased CenKR TCS activity.

Using ChIP-seq analysis, CenR binding was detected upstream of three (*mraZ*, *ftsW*, *ddlA*) of the seven highly conserved promoters within the division and cell wall biosynthesis (*dcw*) gene cluster (*RSP\_2095*–*RSP\_2114*) [58], suggesting that this TCS plays a direct role in repressing the transcription of these genes (S1 Table and S6 Fig). However, these promoter regions did not contain the predicted binding motif for this RR in the vicinity of the known TSS, and no decline in CenR enrichment was detected in strains harboring an inactive TCS (S6 Fig). Therefore, we propose that CenR either requires another DNA binding protein to alter transcription, plays an indirect role in the regulation of these genes through hierarchical regulation of other transcription factors, or this represents an artifact in ChIP-seq analysis. In any case, further experiments are required to resolve this. Related to the differential expression of the *dcw* cluster, other genes encoding PG remodeling proteins such as the lytic transglycosylase *mltB* (increased by CenR activity) and D-alanine-D-alanine carboxypeptidase *dacC* (decreased by CenR activity) [5] were predicted to be indirectly regulated by CenR since they were among our list of DEGs in TCS mutants, but lacked any evidence for binding of this RR by ChIP-seq analysis.

### The CenKR TCS is conserved in $\alpha$ -proteobacteria

Given the high degree of amino acid sequence similarity between *Rb. sphaeroides* and *C. crescentus* CenKR proteins and the impact of altered activity of their respective TCSs on cell shape, we sought to determine if aspects of this system were conserved in other bacteria. To probe the conservation of CenKR in other organisms, we constructed separate maximum-likelihood (ML) phylogenies of both CenK and CenR. The topology of both trees was identical and could be combined (Fig 6, node support for CenK/CenR trees, respectively) into a tree that predicts evolutionary relationships agreeing with other  $\alpha$ -proteobacteria phylogenies [59–62]. From this analysis, we identified homologs of CenK and CenR within eight orders in the  $\alpha$ -proteobacteria phylogeny. These eight formed six, well supported clades consisting of *Rhizobiales* (bootstrap = 98/84), *Hyphomicrobiales* (bs = 98/85) *Caulobacteriales/Parvularculales* (bs = 85/81), *Rhodobacteriales* (bs = 100/98), *Sneathiellales* (bs = 100/100), and *Rhodospirillales/Kiloniellales* (bs = 95/98) representing the *Caulobacteridae* subclass [61,62]. Homologs of CenK or CenR were not identified in organisms belonging to the *Sphingomonadales* (subclass *Caulobacteridae*), orders within the *Rickettsiidae* subclass (encompassing the *Rickettsiales*, *Pelagibacteriales*, and *Holospirales* orders), or the *Magnetococcales* at the base of the  $\alpha$ -proteobacterial phylogeny [59–62], in members of other proteobacterial groups, or elsewhere in the bacterial phylogeny.

The conservation of CenKR homologs in other  $\alpha$ -proteobacteria, as well as the proposed conserved role of the TCS in cell envelope regulation in *C. crescentus* [26] leads us to hypothesize that the genes we identified as direct members of this regulon might also be evolutionarily conserved in other related bacteria. To test this hypothesis, we sought to identify predicted CenR DNA binding sites in the genome of other well-studied organisms such as *Agrobacterium tumefaciens* (*Rhizobiales*), *Brucella abortus* (*Rhizobiales*), *C. crescentus* (*Caulobacteriales*),

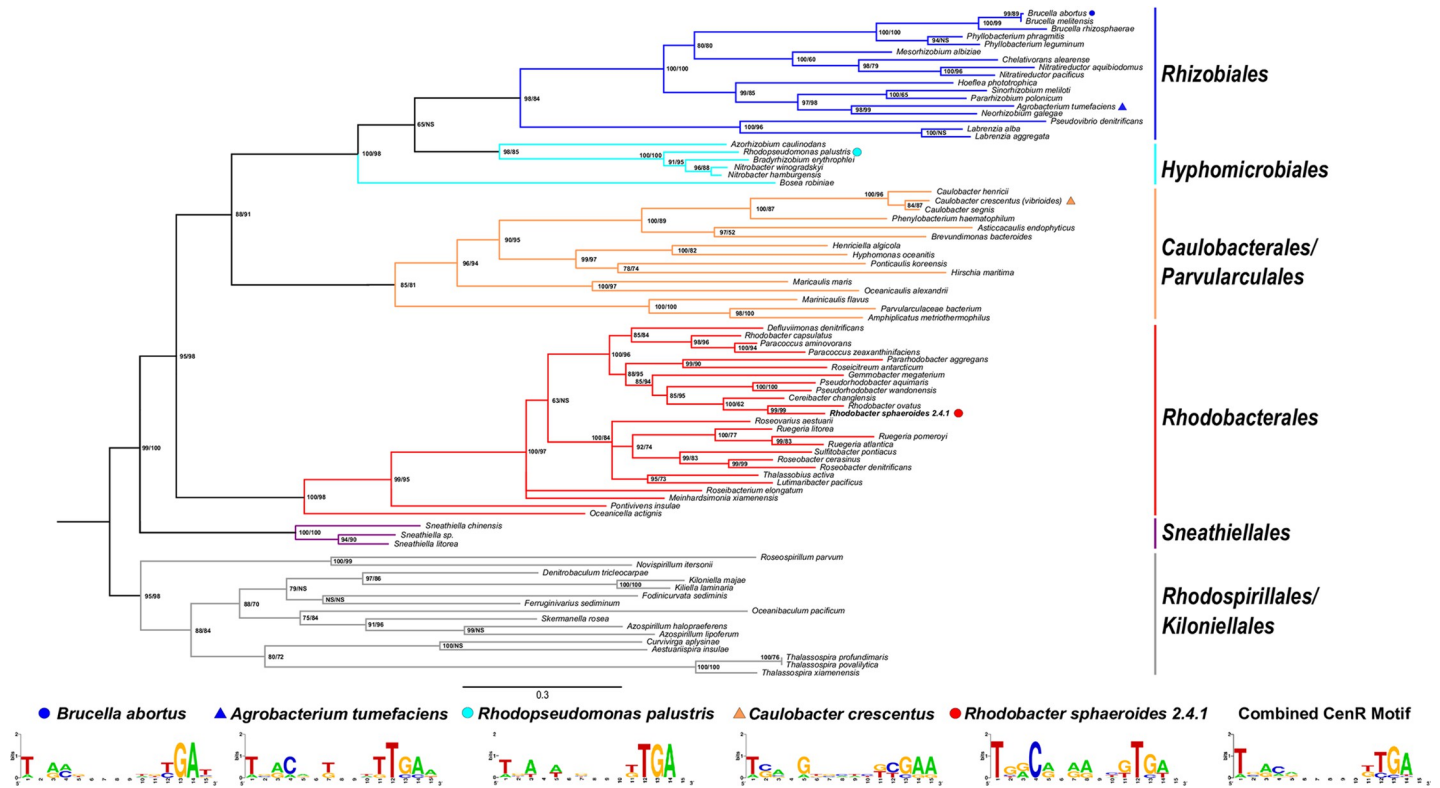


**Fig 6. Homologs of CenKR are found in several other  $\alpha$ -proteobacteria. (Phylogeny)** Combined maximum likelihood phylogenetic tree of CenK and CenR identified in  $\alpha$ -proteobacteria which had identical topologies. Support values (ML bootstrap) for CenK/CenR are listed for each node. Support values under 50 are labeled NS. **(Bottom panel)** Putative sequence logo of the CenR DNA binding motif derived from analyzing the regions upstream of transcriptional units directly controlled by CenR in indicated  $\alpha$ -proteobacteria.

<https://doi.org/10.1371/journal.pgen.1010270.g006>

and *Rhodopseudomonas palustris* (*Hyphomicrobiales*) that contain this TCS. To do so, we compared the mapped CenR binding sites upstream of *cenR*, *tolQ*, *RSP\_1860*, *RSP\_1807*, *surA*, and *msrA* (Table 1) in *Rb. sphaeroides*, with regions 300 bp upstream of each of these operons in these four related species (S4 Table). This analysis identified the conserved direct repeat TGA-N<sub>8</sub>-TGA upstream of each operon in each analyzed species (Fig 6, bottom panel), supporting the hypothesis that CenKR plays a conserved role in cell envelope regulation in  $\alpha$ -proteobacteria.

### Discussion

This work sought to increase our understanding of bacterial cell envelope assembly as well as modifications to this essential cellular compartment. Little is known about these processes in  $\alpha$ -proteobacteria since these organisms lack well-studied regulators of cell envelope processes that are known in other proteobacteria. We showed that the  $\alpha$ -proteobacterium *Rb. sphaeroides* protein RSP\_1056 (CenK) is a HK that phosphorylates an OmpR-family RR, RSP\_0847 (CenR), and these two proteins comprise a TCS with a high degree of amino acid similarity to *C. crescentus* CenKR. We combined genome-scale ChIP-seq with transcript abundance data from cells predicted to have different levels of CenKR activity to identify the direct CenR targets and make predict how this TCS impacts cell envelope functions in this and other  $\alpha$ -proteobacteria (Fig 7). Below we highlight new information provided by our analysis of the *Rb. sphaeroides* CenKR TCS.

## CenKR comprise an essential TCS in *Rb. sphaeroides*

It is known that genes encoding CenK and CenR are essential, encoded at separate loci, and comprise a TCS in *C. crescentus* [26]. In contrast, insertions in *Rb. sphaeroides* *cenK* (*RSP\_1056*) were identified in two separate transposon insertion libraries, suggesting that unlike in *C. crescentus*, this gene is not essential in this  $\alpha$ -proteobacterium [33]. However, the saturating genome-wide transposon library that identified *cenK*, did not contain insertions in *cenR* suggesting that this predicted RR is essential in *Rb. sphaeroides* (S2 Fig) [25]. Similarly, a Tn-seq screen performed in  $\alpha$ -proteobacterium *Rhodospseudomonas palustris* (Fig 6, *Hyphomicrobiales*) identified insertions in the homolog of *cenK* (*RPA0635*), but not *cenR* (*RPA0283*) suggesting that this RR is also essential in this bacterium [63]. To date, only a few bacterial TCSs are known to be essential. Indeed, systematic disruption of the 106 TCS genes in *C. crescentus* identified only four essential TCS pairs. Three of these, CenK-CenR, CtrA-CckA, and DivK-DivJ, are known or predicted to be involved in cell cycle or cell envelope processes [26]. Another essential *C. crescentus* gene identified in this study was *ntrX*, encoding the RR in the NtrYX TCS that regulates LPS, exopolysaccharide synthesis, and cell wall composition in *Rb. sphaeroides* [64]. Other essential TCSs that directly regulate crucial cell wall biosynthesis machinery include WalKR in the Gram-positive organisms *Streptococcus pneumoniae* (also known as VicKR) [65] and *Bacillus subtilis* [66], WigRK in the pathogenic Gram-negative bacterium *V. cholerae* [22], and MtrAB in the pathogenic bacterium *Mycobacterium tuberculosis* [23,24]. In contrast, the cell envelope stress response TCSs Cpx and Rcs in Gram-negative  $\gamma$ -proteobacteria like *E. coli* are not essential and regulate genes that mitigate OM/LPS, OM protein, or lipoprotein stress rather than directly regulating cell envelope biogenesis machinery [11,67].

*C. crescentus* *ntrX*, *M. tuberculosis* *mtrA*, *S. pneumoniae* *vicR* (*walR*), and *Rb. sphaeroides*/*C. crescentus* *cenR* each are examples of essential RRs linked to non-essential HKs, suggesting that loss of the HK reduces TCS activity and that these RRs have some critical function in the absence of phosphorylation [24,26,65]. Supporting this, our *in vivo* analysis of a *cenR*(D56A) allele that abolishes phosphotransfer between CenK and CenR *in vitro* (Fig 1D) suggests that this mutation diminishes CenR activity as the *cenR*(D56A) allele phenocopies the  $\Delta$ *cenK* strain (Fig 2). Furthermore, in strains with low CenKR activity ( $\Delta$ *cenK* and *cenR*(D56A)), we detected CenR binding to some promoters by ChIP-seq (Fig 5A). Based on these observations, we propose that CenR has basal activity in the absence of phosphorylation that is sufficient to promote transcription of essential genes and/or pathways, comparable to other TCS [32,65].

## *Rb. sphaeroides* CenKR regulates essential division, cell wall, and other envelope processes

Genetic and biochemical characterization of *Rb. sphaeroides* CenKR allowed us to identify direct and indirect targets of this TCS. Our data predict that most members of the direct CenR regulon encode proteins that contain signal peptides and are predicted to be targeted to the OM or periplasmic space. These direct CenKR regulon members prominently included predicted OM structural or transport proteins, PG binding proteins, and periplasmic chaperones or proteases. Of the genes predicted to be direct targets of CenR, ~42% are annotated as either hypothetical proteins or have generic descriptions of their function, thus we propose these represent candidates for the future study of envelope components that are controlled by the CenKR TCS. For example,  $\alpha$ -proteobacteria lack homologs of the well-studied spatial regulators of *E. coli* PG biosynthesis LpoA and LpoB [57,68], so it is possible that one or more members of the CenKR direct regulon provide this function. Our data also predict that CenR indirectly regulates genes encoding PG biosynthesis enzymes that promote lateral cell wall

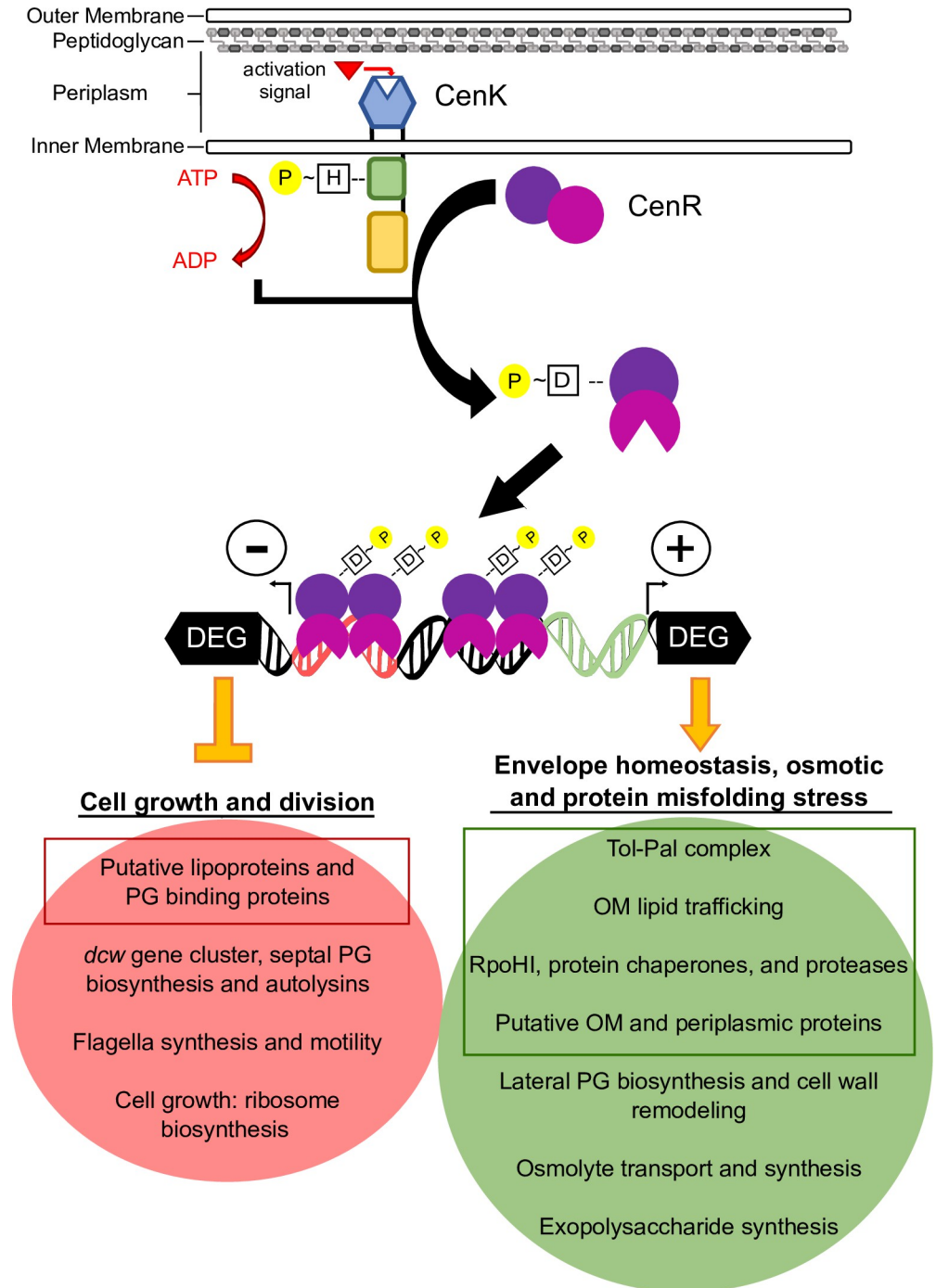


**Fig 7. Model for the cellular impacts of direct and indirect CenKR transcriptional regulation.** CenK autophosphorylation occurs at a conserved histidine residue within its cytoplasmic domain in response to an unknown signal. CenK then phosphorylates CenR at aspartate 56 within the receiver domain, resulting in conformational changes that allow CenR to bind the promoter regions of direct target genes, repressing transcription by binding within the promoter elements (red) or activating transcription by binding upstream of promoter elements (green). Phosphorylated CenR directly upregulates (green box) genes and pathways that function in the mitigation of cellular or cell envelope stresses, maintenance of the envelope, the Tol complex that plays a vital role in OM division and stability, and other genes of unknown function predicted to be involved in the assembly or repair of cell envelope components. Indirectly, increased activity of CenR results in the increased expression of genes that function in an osmotic stress response and synthesis/remodeling of lateral cell wall (green oval). Phosphorylated CenR directly reduces transcription (red box) of gene products of unknown function that are predicted to be targeted to the cell

envelope. Indirectly, increased activity of CenR decreases expression of genes within the *dcw* gene cluster that function in septal PG and cell wall biosynthesis, and genes whose products cleave PG, synthesize flagellar, and are vital for cell growth such as ribosome biosynthesis (red oval).

<https://doi.org/10.1371/journal.pgen.1010270.g007>

synthesis (Fig 5D). This, plus the observed changes in cell shape when CenKR activity is increased or decreased (Fig 2A–2C) make testable predictions that one or more direct, or indirect, targets of CenKR may have a role in the spatial regulation of cell wall synthesis. Given the relatively thin cell wall of Gram-negative bacteria, precise control of PG synthesis, turnover, and repair is essential, and in other bacterial cells, redundant pathways exist to maintain cell wall integrity in response to environmental signals and membrane-active agents [5]. Furthermore, the number of PG cleavage or crosslinking enzymes (amidases, lytic transglycosylases, carboxypeptidases, and D,D-endopeptidases or D,D/L,D-transpeptidases and glycosyltransferases) vary among bacteria [50,51]. *Rb. sphaeroides* contains nine predicted lytic transglycosylases and nine predicted L,D-transpeptidases compared to the eight and six, respectively, that have been identified in *E. coli* [50,51]. Our datasets identify *Rb. sphaeroides* candidates for gene products that may fill some of these roles or occupy other cellular niches including *RSP\_1199*, annotated to encode a predicted L,D-transpeptidase (upregulated by CenKR), and *RSP\_1880*, encoding a putative PG binding protein that may have autolytic activity since it is downregulated by CenKR. Thus, we predict that analyzing genes that are direct or indirect CenKR targets will shed new light on the process and control of PG biosynthesis across  $\alpha$ -proteobacteria.

We also identified CenR as a direct regulator of the Tol subunits of the Tol-Pal complex (Fig 5A), a system that has been implicated in envelope processes such as OM migration during septal constriction [69,70], coordination of PG remodeling/cleavage at the site of cell division [71,72], and polar localization of proteins [73]. It has also been proposed that Tol-Pal is important for maintaining noncovalent OM-PG interactions in Gram-negative bacteria like *Rb. sphaeroides* that lack a homolog of the Braun's lipoprotein [74]. Recently, it has been shown that the function of Braun's lipoprotein in  $\alpha$ -proteobacteria is facilitated by other OM  $\beta$ -barrel proteins that are covalently bound to PG through the activity of L,D-transpeptidases in  $\alpha$ -proteobacteria [74]. Given the effects of disruption of Tol-Pal on OM integrity, leakiness, and OM vesicle production in other organisms [75], we propose that Tol-Pal, or Tol-Pal associated proteins, may coordinate one or more of these processes in  $\alpha$ -proteobacteria. In other bacteria, a reduction or loss of Tol-Pal components also increases cell permeability and OM fluidity due to an increase in OM phospholipid and a reduction or loss of LPS [75,76]. This also appears to be the case in *Rb. sphaeroides* since disruption of *cenK* resulted in increased cellular phospholipids, lipid secretion, and enhanced sensitivity to detergents (like SDS and polymyxin B) which are normally excluded by LPS [25]. We also found that cells containing a phosphomimetic *cenR* allele, *cenR*(D56E), that is predicted to increase activity of this TCS *in vivo*, resulted in cell filamentation, suggesting that CenKR activity coordinates cell division and/or cytokinesis.

It is known that *tol* operon genes encoding IM subunits of the Tol complex are essential in *Rb. sphaeroides*, *C. crescentus*, and other  $\alpha$ -proteobacteria [73,77]. In other bacteria where the Tol system has been well-studied, the IM Tol complex (TolQRA) facilitates Pal localization and PG binding at the septum during cell division, by regulating the interaction between the OM lipoprotein Pal and the periplasmic TolB protein [70,78]. In *E. coli* and related organisms, *tolQRA* and *tolB-pal-cpoB* make up two transcriptional units [79]. However, in *Rb. sphaeroides*, *C. crescentus*, and other  $\alpha$ -proteobacteria *tolB* is part of the *tolQRAB* transcriptional unit, and *pal-cpoB* are in a separate transcriptional unit [41,73]. Our analysis indicates that CenR acts

directly at *tolQRAB* but, does not directly or indirectly regulate the expression of *pal-cpoB* (Fig 5A). As the function of Pal and TolQRAB are proposed to be essential in several  $\alpha$ -proteobacteria [33,63,73,75], we propose that organisms with the same *tol-pal* synteny rely on CenKR to regulate the activity of Tol-Pal by direct control of *tolQRAB* transcription. Such a mechanism would allow for the regulation of essential Tol driven cell division processes while allowing Pal to maintain other functions independent of the subunits of Tol.

The many roles of Tol-Pal complex as well as the essential role of this machine in several  $\alpha$ -proteobacteria [73,75,77] likely contributes to CenR essentiality and further supports our hypothesis that CenKR regulates functions necessary for cell division. To our knowledge, CenKR is the first TCS in Gram-negative bacteria that directly regulates genes encoding Tol complex proteins. Mutations that impact the *E. coli* Rcs are reported to increase expression of the Tol-Pal genes [80], and inactivation of the *C. crescentus* ChvGI altered expression of genes encoding subunits of the Tol-Pal complex [15]. However, it is unclear in these organisms if these TCSs directly or indirectly regulate the expression of these genes.

### The CenKR TCS also controls cellular stress responses

We identified CenR as a direct activator of *rpoHI* expression (Fig 5B), one of two *Rb. sphaeroides*  $\sigma^{32}$  alternate sigma factors, that control transcription of gene products that function in protein quality control and turnover, ion transport, and oxidative stress responses (i.e. disulfide bond and peroxide reduction) [54,81]. Previously, it was proposed that CenR negatively regulates *rpoHI* expression [54]. However, we found reduced levels of transcripts of both *rpoHI* and known RpoHI regulon members in cells containing low CenKR activity ( $\Delta cenK$  or *cenR*(D56A)) and increased levels of these transcripts in cells containing increased activity of this TCS (*cenR*(D56E)). Direct activation of *rpoHI* transcription by CenR suggests that CenKR activates expression, in a hierarchical fashion, of a large set of genes that encode proteins functioning to mitigate general, cytoplasmic, or membrane stress responses.

The *E. coli* RseA- $\sigma^E$  system is another master regulator of both unique genes encoding proteins with cell envelope functions and some genes which also are members of the Cpx or Rcs regulons, thereby functioning broadly to monitor extracytoplasmic homeostasis [11,67]. In *E. coli* it is proposed that accumulation of unfolded or mislocalized OM proteins activates proteases that degrade the anti- $\sigma^E$  factor RseA, allowing  $\sigma^E$  to promote transcription of envelope stress response genes [78]. *Rb. sphaeroides* lacks homologs of *E. coli* RseA- $\sigma^E$ , but it is known that RpoHI is a direct regulator of *cenR* transcription in response to heat shock, oxidative and/or membrane stress signals [54,82]. Thus, we propose the existence of a positive CenR-RpoHI feedback loop that allows a robust, synergistic response to agents that act at the cell envelope. Given the lack of homologs of *E. coli* Cps, Rcs, and RseA- $\sigma^E$  in *Rb. sphaeroides* and other  $\alpha$ -proteobacteria, it is likely that CenKR is a major contributor to a transcriptional response to envelope derived signals.

Other likely indirect effects of changes in CenKR activity include repression of genes involved in chemotaxis, motility, flagellar machinery, and those encoding ribosomal proteins, the latter is consistent with the slow growth rate of strains harboring the hyperactive CenR (D56E) protein (S2 Data). Low CenKR activity in  $\Delta cenK$  or *cenR*(D56A) is also associated with an increase in transcripts from genes encoding proteins that function in polysaccharide production, sarcosine/glycine biosynthesis, and transport of osmolytes which, together, mitigate osmotic stress within the cell [83] and the periplasmic space [84]. Given the role of the OM LPS and the cell wall in resistance to turgor pressure [3] and the altered levels of transcripts from genes whose products are predicted to function in assembly or maintenance of these structures in cells with low CenKR activity, we propose this results in the responsive expression

of these osmotic stress response genes. Together, the CenKR TCS is a heretofore unknown regulator of cell envelope changes necessary to combat internal/external turgor pressures.

### The presence and role of CenKR is predicted to be conserved across $\alpha$ -proteobacteria

We identified homologs of CenK and CenR within the *Caulobacteridae* sub-class of  $\alpha$ -proteobacteria, including free-living, commensal, and pathogenic organisms. Many of the  $\alpha$ -proteobacteria that contain CenKR homologs undergo morphological changes throughout their lifecycle. Purple non-sulfur bacteria like *Rb. sphaeroides* and *Rp. palustris*, under low oxygen conditions, produce intracytoplasmic membranes as cell envelope invaginations that bud inward from the IM and house the machinery for the light reactions of photosynthesis [85,86]. *C. crescentus* and *Rp. palustris*, and other members of the *Rhizobiales* that contain CenKR homologs, have a dimorphic life cycle that requires changes in cell envelope, loss of flagella, and the formation of stalks that differentiate free-living swarmer cells to an anchored sessile form [87,88]. The animal parasite *B. abortus* relies on membrane changes for macrophage internalization and pathogenesis [89], and the plant pathogen *A. tumefaciens*, as well as other members of the *Rhizobiales*, exhibit polar growth and utilize polar budding for division and exhibits a range of morphologies when cell division is altered [90]. These examples showcase some of the cell envelope and cell cycle alterations that are characteristic of  $\alpha$ -proteobacteria containing CenKR homologs. We propose that these lifestyles are one reason why these organisms contain cell envelope TCSs and stress response machinery different from those classically studied in *E. coli* and other bacteria. We note that we were unable to identify homologues of CenKR in the *Sphingomonadales* or *Rickettsiales* clades (Fig 6),  $\alpha$ -proteobacteria that are known to exhibit unusual cell envelope features. *Sphingomonades* contain sphingolipids in the outer leaflet of the OM rather than LPS [91], and members of the *Rickettsiales* include many obligate parasitic bacteria that lack complete cell wall biosynthetic pathways or known membrane-bound enzymes to polymerize PG precursor molecules into the nascent cell wall [92,93]. The existence of CenKR across the *Caulobacteridae* subclass of  $\alpha$ -proteobacteria supports a hypothesis that this TCS coordinates a myriad of activities that reside in the OM, LPS, or PG cell wall. There is no recognizable ligand-binding domain in the N-terminal periplasmic or IM region of the CenK HK, so further experiments are needed to identify the signal(s) that controls CenK kinase activity to determine if CenKR responds to signals derived from these cell envelope components.

In closing, we have shown that CenKR is one of several identified TCSs that regulates cell envelope homeostasis in  $\alpha$ -proteobacteria [15,64]. However, the function(s) of these other recently identified cell envelope regulators are not necessarily conserved across  $\alpha$ -proteobacteria. For example, NtrYX has been implicated as a regulator of root nodule formations that are involved in nitrogen fixations, carbon/nitrogen metabolism, transport systems [94–96], regulation of anaerobic processes [95,97,98], as well as exopolysaccharide biosynthesis, cell envelope composition, and growth [15,64,95,99]. Similarly, in some  $\alpha$ -proteobacteria, ChvIG has been linked to growth [15], pathogenesis [100,101], motility [102], and pH sensitivity [103]. In contrast, the presence of a putative *Rb. sphaeroides* CenR binding motif (TGA-N<sub>8</sub>-TGA), upstream of several conserved transcriptional units across  $\alpha$ -proteobacteria (including the *tol* operon), suggests a similar role for the CenKR in these species. While further study of the signals that control CenKR kinase and DNA binding activity are required to better understand the role of this TCS, we have shown that CenKR is an essential TCS, defined the regulon controlled by this regulatory system, and we predict that it plays a conserved and central role

in envelope, cell division, and other processes that are crucial to viability in *Rb. sphaeroides* and other  $\alpha$ -proteobacteria.

## Materials and methods

### Bacterial strains and growth conditions

*Rb. sphaeroides* strains (S2 Table) were grown in Siström's (SIS) minimal medium [104]. Unless specified, aerobic cultures of 10 mL were grown in 125 mL flasks with shaking at 200 rpm, at 30°C for ~18 hours until cells reached an OD<sub>600</sub> of ~0.5. *Escherichia coli* strains were grown at 37°C in Luria-Bertani medium. As needed, media was supplemented with 50 µg/mL kanamycin, 25 µg/mL spectinomycin, or 10 µM isopropyl β-D-1-thiogalactopyranoside (IPTG).

### Strain construction

All strains, primers, and plasmids used in this study are listed in S2A and S2B Table). In-frame, markerless deletion of *RSP\_1056* and allelic exchange within *RSP\_0847* was performed via the integration of the suicide vector pk18mobsacB [105]. The genomic regions corresponding to ~1 Kb immediately upstream of the start and downstream of the stop codons of each gene was PCR amplified using Herculase II Fusion DNA Polymerase (Agilent). These PCR products were assembled into PCR linearized pk18mobsacB via Gibson Assembly (New England BioLabs), transformed in DH5α cells (New England BioLabs), and screened by colony PCR of the cloning site and sequenced. Assembled plasmids were mobilized into *Rb. sphaeroides* via conjugal mating with *E. coli* S17-1 [106]. Single crossover transconjugants were selected for by kanamycin resistance followed by sucrose counter-selection to induce double crossovers. Strains with the desired double crossover were identified by isolation of colonies sensitive to kanamycin and resistant to sucrose (S2A Fig). The locus-specific genotype of each strain was confirmed by colony PCR of chromosomal loci and sequenced with specific primers (S2 Table). Construction of pIND5<sub>spec</sub>-*cenR* was achieved by co-transformation of PCR amplified *cenR* and linearized pIND5<sub>spec</sub> into *E. coli* DH5α (New England BioLabs). Assembled plasmids were mobilized into *Rb. sphaeroides* via conjugal mating with *E. coli* S17-1 [106]. Markerless deletion of *RSP\_0847* was attempted in the presence of pIND5<sub>spec</sub>-*cenR* as described above except in the presence of spectinomycin antibiotic and IPTG through the selections.

### Microscopy

All strains were grown as described above to an OD<sub>600</sub> ~ 0.5. Images were acquired on an EVOS FL microscope with 100X oil immersion plan apochromat objective (numerical aperture, 1.40). To facilitate cell segmentation, all bright-field pictures were treated in FIJI [107] with the same process: bandpass filter (large filter, 40 pixels (pxs); small filter, 2 pxs), background subtraction (rolling ball radius = 20 pxs), and contrast enhancing with normalization (0.1%). Segmentation was performed using the plugin MicrobeJ [108] and cell segmentation errors were removed. Cell shape parameters were extracted (S3 Data), figures and statistical analysis were performed in Rstudio using ggplot2 package [109].

### Protein purification and RSP\_0847 (CenR) antibody production

The cytosolic domains of the *RSP\_1056* (CenK) coding sequence (truncated after the second predicted transmembrane helix at residue M195) was PCR amplified and ligated into linearized pVP302K [110] via HiFi Gibson Assembly (New England BioLabs), generating an N-

terminal His<sub>8</sub>-tagged protein containing a TEV protease cleave site (H<sub>8</sub>-TEV-HK<sub>cyto</sub>). Candidate RR genes (RSP\_0847, RSP\_1083, RSP\_1247) were ligated into the same expression vector containing a C-terminal His<sub>8</sub> tag and TEV cleavage site (RR-TEV-H<sub>8</sub>). Candidate TCS expression plasmids were transformed into B834 *E. coli* harboring pRARE2 (Novagen) [111,112]. Cells were grown in 500 mL of ZMS-80155 auto-inducing media supplemented with 10 µg/mL kanamycin and 20 µg/mL chloramphenicol for ~24 hours with shaking at room temperature. Cells were harvested by centrifugation, resuspended in 10 mL of lysis buffer (20 mM HEPES-KOH [pH 7.5], 0.5 M NaCl, 5 mM imidazole, 1% glycerol, 1 mM TCEP, 0.1% Triton X-100) and 100 µL of HALT Protease Inhibitor (Thermo), lysed by sonication, and centrifuged at 4°C for 30 min at 20,000 x *g* to generate a lysate. The lysate was added to 5 mL washed Ni-NTA agarose slurry (Qiagen) and loaded into a gravity-flow column (BioRad). After passaging the lysate, the column was washed with 2 column volumes of wash buffer (20 mM HEPES-KOH [pH 7.5], 500 mM NaCl, 40 mM imidazole, 1 mM TCEP, 1% glycerol) and protein was eluted with 10 mL elution buffer (20 mM HEPES-KOH [pH 7.5], 300 mM NaCl, 400 mM imidazole, 1 mM TCEP, 1% glycerol). Fractions containing the most protein were combined and concentrated using a YM10 centrifugal filter (Millipore) before being dialyzed using a 10,000 molecular weight cut-off Slide-a-Lyzer dialysis cassette (Thermo Scientific) into storage buffer (20 mM HEPES-KOH [pH 7.5], 300 mM NaCl, 50 mM KCl, 1 mM TCEP, 5% glycerol, 0.1 mM EDTA). Protein was aliquoted and stored at -80°C. Protein concentration was estimated using the Bradford Assay (Bio-Rad).

To obtain RSP\_0847 for antibody production (used in ChIP-seq), after dialysis of RSP\_0847-TEV-H<sub>8</sub>, the H<sub>8</sub> tag was cleaved by incubation with H<sub>6</sub>-TEV protease. The cleaved H<sub>8</sub> tag and H<sub>6</sub>-TEV protease were removed with a second round of Ni-NTA chromatography. A 5 mL RSP\_0847 protein fraction was subjected to size exclusion chromatography in storage buffer through a GE Healthcare HiLoad 16/600 Superdex 75 pg 120mL XK column (Millipore) at a flow rate on 0.5 mL/min controlled by a GE Healthcare ÄKTA Prime Plus FPLC system. Two mL fractions were collected, and sample purity was analyzed by loading ~250 ng of protein on a 12% SDS-PAGE gel. Fractions enriched for RSP\_0847 (MW = 28.2 kDa) were combined and concentrated, as above, to ~2 mg/mL. Purified RSP\_0847 protein was sent to Covance (Denver, PA) to raise a rabbit polyclonal antibody.

### Phosphotransfer assay

Purified, truncated RSP\_1056 (5 µM) was incubated at 30°C for 30 minutes in storage buffer supplemented with 50mM Tris-HCl pH 7.5, 50 mM KCl, 5 mM MgCl<sub>2</sub>, 50 µM ATP, 1 µCi [ $\gamma$ <sup>32</sup>P] ATP (6.16 µCi/µL, [Perkin Elmer]). Purified candidate response regulator proteins were diluted to 5 µM in storage buffer. For each phosphotransfer assay, 5 µL phosphorylated kinase (from the above reaction) and 5 µL response regulator (2.5 µM each protein in storage buffer) were incubated at 30°C. Reactions were stopped with 5 µL 3x NuPAGE LDS (Thermo Fisher) containing 10 mM DTT and stored on ice until samples were loaded, without heating, onto a NuPAGE 4–12% Bis-Tris Protein gel (Invitrogen). Samples were electrophoresed at room temperature for 50 minutes at 150 V. Regions of the gel below the dye front were removed with a razor blade, and the gel was placed between saran wrap and dried for 30 minutes. The dried gel was exposed to a phosphor screen for 3 hours at room temperature before imaging with a Typhoon phosphorimager at 50 µm resolution.

### RNA isolation and sequencing

*Rb. sphaeroides* was grown aerobically in 500 mL cultures bubbled with 69% N<sub>2</sub>, 30% O<sub>2</sub>, and 1% CO<sub>2</sub>. 44 mL of cells were harvested when the culture reached an OD<sub>600</sub> of ~0.5 (mid-log),

combined with 6 mL of ice-cold stop solution (95% EtOH and 5% acid phenol:chloroform (5:1, pH 4.5)), and centrifuged at 4°C for 10 minutes at 6,000 x g. Cell pellets were resuspended in 2 mL of lysis solution (2% sodium dodecyl sulfate, 16mM EDTA, RNase-free water) and heated at 65°C for 5 minutes. Nucleic acids were extracted using 2 mL of acidic phenol:chloroform heated to 65°C, mixed by inversion, incubated at 65°C for 5 minutes, and centrifuged at room temperature for 7 minutes at 20,000 x g. The aqueous phase was removed, extracted twice more, before addition of 2 mL of chloroform, mixed, and centrifuged once more at room temperature for 7 minutes at 20,000 x g. The aqueous layer was removed and mixed with 1/10 volume of 3M sodium acetate and equal volume of isopropanol, and incubated at -20°C for >1 hour to precipitate nucleic acids that were collected by centrifugation at 4°C for 30 minutes at 16,000 x g. The pellet was washed twice with 1 mL of 75% EtOH (prepared with RNase-free water). Once residual ethanol was removed by evaporation, the pellet was resuspended in 85 µL of RNase-free water. Samples were treated with RNase-free DNase (10 µL 10x DNase buffer, 2 µL DNase, 3 µL RNasin (Promega)) and purified using RNeasy kit (Qiagen).

RNA-seq library preparation and sequencing were performed at the Joint Genome Institute. Sequencing libraries were created using the Illumina TruSeq Stranded Total RNA kit (Illumina) and sequenced on an Illumina NextSeq in 2x151 reads using the manufacturers protocol. The resulting paired-end FASTQ files were split into R1 and R2 files, and R1 files were retained for processing through the same pipeline. Reads were trimmed using Trimmomatic version 0.3 [113] with the default settings except for a HEADCROP of 5, LEADING of 3, TRAILING of 3, SLIDINGWINDOW of 3:30, and MINLEN of 36. After trimming, the reads were aligned to the *Rb. sphaeroides* 2.4.1 genome sequence (GenBank accession number GCA\_000012905.2) using Bowtie2 version 2.2.2 [114] with default settings except that the number of mismatches was set at 1. Aligned reads were mapped to gene locations using HTSeq version 0.6.0 [115] using default settings except that the “reverse” strandedness argument was used. edgeR version 3.26.8 [116,117] was used to identify significantly differentially expressed genes from pairwise analyses, using Benjamini and Hochberg [118] false discovery rate (FDR) of less than 0.05 as a significance threshold. Raw sequencing reads were normalized using the reads per kilobase per million mapped reads (RPKM). Pathway enrichment was performed using the SmartTable enrichment function at [biocyc.org](http://biocyc.org) [119] using a P value of  $\leq 0.05$  as significant.

### Chromatin immunoprecipitation, sequencing, and CenR binding site analysis

*Rb. sphaeroides* strains (S2 Table) were grown aerobically in 500 mL culture bubbled (69% N<sub>2</sub>, 30% O<sub>2</sub>, and 1% CO<sub>2</sub>). To each 500 mL culture, 5 mL of 1M sodium phosphate mix (0.85 M Na<sub>2</sub>HPO<sub>4</sub>, 0.15 M NaH<sub>2</sub>PO<sub>4</sub>) and 13 mL of 37% formaldehyde was added. Crosslinking was allowed to continue with continuous bubbling of the culture for 5 minutes. Each culture was placed into an ice bath and 20 mL of ice cold 2.5 M glycine was added and incubated with bubbling for 30 minutes to quench crosslinking. Cells were pelleted in 50 mL portions by centrifugation at 3500 x g for 10 minutes at 4°C, washed twice with 100 mL of phosphate buffered saline (PBS), resuspended in 1 mL of PBS, and flash frozen. DNA was isolated in tandem and pooled from technical replicates to improve DNA yields. For DNA isolation, cell pellets were resuspended in 500 µL RIPA buffer (Sigma) supplemented with 50 µL HALT Protease Inhibitor (Thermo). Cells were lysed at 4°C by water bath sonication for 30 cycles at 25% pulsed 25 seconds on and 35 seconds off. To each lysate, 2 µL of micrococcal nuclease (Pierce), 10 µL CaCl<sub>2</sub> mix (15 mM Tris-HCl pH 8, 1 mM CaCl<sub>2</sub>, 60 mM KCl, 15 mM NaCl, 300 mM sucrose, 0.5 mM DTT), and 10 µL RNase A (0.1 mg/mL final (Fisher)) was added and the mixture was

incubated at 4°C for 1 hour. Each nuclease reaction was stopped with 15 mM EDTA and lysate was centrifuged at 16,000 x g at 4°C to remove cell debris. DNA fragmentation (major band between 200-400bp) was checked by gel electrophoresis on a 1.5% agarose gel. For immunoprecipitation, 1/10 of the volume was taken from each lysate and mixed with an equal volume Protein A sepharose beads (Sigma) to be used as input and negative control. After preclearing the remaining lysate volume with 50 µL Sepharose beads, 5 µL of polyclonal anti-RSP\_0847 antibody was added to each sample and incubated at 4°C overnight. Sepharose beads (60 µL) were added to each lysate, the volume was adjusted to ~750 µL with RIPA buffer, and samples were centrifuged for 2 minutes at 1,000 x g at 4°C to pellet antibody-protein-DNA complexes bound to the beads. The pelleted beads were washed twice with 1 mL LiCl Wash Solution (100 mM Tris-HCl pH 8, 250 mM LiCl, 2% TritonX-100), twice with 1 mL 600 mM NaCl Wash Buffer (100 mM Tris-HCl pH 8, 600 mM NaCl, 2% TritonX-100), twice with 1 mL 300 mM NaCl Wash Buffer (100 mM Tris-HCl pH 8, 300 mM NaCl, 2% TritonX-100) and twice with TE Buffer (10 mM Tris-HCl pH8, 1 mM EDTA). 150 µL Elution Buffer (50 mM Tris-HCl pH 8, 10 mM EDTA, 1% SDS) was added to the pelleted Sepharose beads and incubated for 1 hour at 65°C. The mixture was centrifuged (1,000 x g at 4°C) and the supernatant was removed and incubated overnight at 65°C to reverse-crosslinking. DNA was purified using QIAquick PCR Purification Kit (Qiagen), eluted into a volume of 50 µL and quantified using Qubit Fluorometer 1x dsDNA HS kit (Invitrogen, CA) for sequencing.

ChIP-seq library preparation (starting with at least 20 ng DNA per sample) and sequencing was performed by GeneWiz (South Plainfield, NJ) using an Illumina ChIP-seq Library kit for sequencing with Illumina HiSeq 2x150 bp configuration, single index. The paired-end FASTQ files were trimmed with Trimmomatic version 0.3 [113] with default settings except for LEADING:3, TRAILING:3, SLIDINGWINDOW:3:30, and MINLEN:36. The trimmed paired-end reads were aligned to the *Rb. sphaeroides* genome sequence (GenBank accession Chr1: NC\_007493.2, Chr2: NC\_007494.2) using Bowtie2 version 2.2.2 [114] with default settings except the number of mismatches was set to 1. Picard-tools version 1.98 [120] and Samtools version 1.2 [121] were used to clean, sort, and index the alignment file using default settings. Areas of enrichment of immunoprecipitated over INPUT (peaks) were identified using MOSAiCS version 2.28 using two factor analysis and an analysis type of "IO" [122]. Conversion of BAM to ELAND format for MOSAiCS was performed using Pyicos version 2.0.6 [123] and default settings. WIG files were generated for each sample using QuEST version 2.4 [124] and default settings. WIG files were visualized on MochiView version 1.46 [125].

To identify a potential consensus CenR binding site, sequences 200bp upstream of the translational start site of candidate transcriptional units (S1 Table) were selected and MEME [42,43] was used to search for an enriched motif present in these 59 sequences using the following parameters: -objfun classic -dna -mod zoops -minw 10 -maxw 20 -allw -revcomp. The PWM (S4B Table) generated from this alignment was used to produce the candidate CenR motif (Fig 4A, E-value 2.6e-10). MEME identified this motif in 31 sequences with a p-value < 0.001 for each individual sequence. Orientation and proximity of each candidate sequence to mapped TSS [41] and predicted promoter elements [126] was assessed within the *Rb. sphaeroides* 2.4.1 genome.

## Electromobility Shift Assays

DNA fragments (250-300bp) were PCR amplified from genomic DNA and purified via gel excision (Qiagen). H<sub>8</sub>-TEV-CenR was purified as described above and the H<sub>8</sub> tag was cleaved with H<sub>6</sub>-TEV protease and removed via gravity flow nickel agarose column. 20 µM CenR was phosphorylated in storage buffer supplemented with 25 mM acetyl-phosphate and 20 mM

MgCl<sub>2</sub> and incubated at 37°C for 1.5hrs. EMSA reactions (10 μL total) consisted of a final concentration of 25 mM Tris-HCl pH 7.9, 5 mM EDTA, 10% glycerol, 40 mM potassium glutamate, 20 μg/mL BSA, 1 mM DTT, 200 mM NaCl, and 15 nM DNA substrate. Appropriate dilutions of phosphorylated CenR were made in storage buffer and 1 μL was added to each reaction for a final monomer protein concentration indicated in the figure. Reactions were incubated at 30°C for 30 min, stopped by addition of 5x loading dye (Invitrogen), and loaded onto a 6% nondenaturing polyacrylamide TBE gel, and electrophoresed in 0.5x TBE with 10% glycerol for 2 hours at 100V. Following electrophoresis, the gel was stained with SYBR green (Invitrogen) 1:10,000 in 1x TBE for 30 min in the dark and imaged on a Visi-Blue transilluminator.

### Phylogenetic analysis and identification of CenR binding sites in other *Alphaproteobacteria*

Amino acid sequences of RSP\_1056 (CenK) and RSP\_0847 (CenR) were used from the *Rb. sphaeroides* 2.4.1 genome (Genbank accession numbers ABA80240.1 and ABA80028.1, respectively) and homologs in other  $\alpha$ -proteobacteria were identified via BLASTP of non-redundant sequences in Genbank (E-value > 1e-70 with a percent identity match >30%) [127,128]. Gene sequences were then aligned in MEGA version 6.06 [129] using MUSCLE [130] and trimmed using Gblocks [131]. Phylogenetic trees were constructed using the Maximum-Likelihood (ML) methods of analysis. The ML analyses for all genes were performed using FastTree 2 [132] with the parameters: -wag, -gamma, -pseudo. Bootstrap values (bs) are reported for the ML trees. Trees were rooted with the *Rhodospirillales* clade to match established  $\alpha$ -proteobacteria relationships [59–62]. Trees were colored by order: Grey–*Rhodospirillales/Kiloniellales*; Purple–*Sneathiellales*; Red–*Rhodobacterales*; Orange–*Caulobacterales/Parvularculales*; Cyan–*Hyphomicrobiales*; Blue–*Rhizobiales*.

To investigate possible CenR regulation in other  $\alpha$ -proteobacteria, we identified potential homologs of *R. sphaeroides* CenR regulated genes in four well studied organisms: *C. crescentus* (NA1000, RefSeq accession number GCF\_000022005.1), *B. abortus* (2308, RefSeq accession number GCF\_000054005.1), *A. tumefaciens* (BIM B-1315G, RefSeq accession number GCF\_014489975.1), and *Rp. palustris* (RCB100, RefSeq accession number GCA\_000195775.1). Homologs were identified using BLASTn (version 2.9.0, default settings) [127,128]. For each identified homolog from each organism, 300 bp upstream of the translation start site was selected and searched for a match to the *Rb. sphaeroides* CenR PWM using PatSer (version 3f, default settings) [133]. For each sequence, the single site with the highest PatSer score was retained. Logos were constructed from the PatSer identified CenR sites using WebLogo [134].

### Supporting information

**S1 Fig. Other predicted partners of CenK are not phosphorylated *in vitro*.** (A) Bayesian probabilities for the highest ranked predicted cognate response regulator of RSP\_1056. Reciprocal search of this database for cognate kinases of RSP\_0847 also identified RSP\_1056 as the highest ranked partner. The Bayesian algorithm models amino acid composition of interacting kinase/regulator pairs to predict specific interaction networks for orphaned TCSs across bacterial genomes [27]. (B) Phosphotransfer between phosphorylated RSP\_1056 and the candidate recombinant response regulators RSP\_1083 and RSP\_1274 was not detected. (PDF)

**S2 Fig. Use of pk18mobsacB- $\Delta$ cenR supports essentiality of this RR in *Rb. sphaeroides*.** (A) Schematic for the workflow of recombineering in *Rb. sphaeroides*. Cloned into the suicide

vector, pk18mobsacB, are 1kb DNA fragments corresponding to the sequences immediately 5' (upstream) and 3' (downstream) of the desired recombination site. Following successful mating, stable integration of the plasmid into the genome by recombination is selected for first by resistance to kanamycin. The second crossover is initiated by counter selection with sucrose as cells harboring *sacB* do not survive in the presence of sucrose. Thus, a successful double crossover is identified by screening for Kan<sup>S</sup>Suc<sup>R</sup> colonies. This double crossover can occur at either the original integration site resulting in no change to the chromosome or within the second homologous region resulting in allelic exchange within the target region. **(B)** Deletion of *cenR* is possible in the presence of an ectopic copy of *cenR*. The results of colony PCR screening for the loss of *cenR* (lane 1–3) in strains containing pIND5<sub>spec</sub>-*cenR* (lanes 4–6) relative to WT (lanes 3,6). Colony 1 represents the first possible outcome of the double crossover workflow and colony 2 represents the second possible outcome and successful deletion of *cenR*. **(C)** Deletion of *cenR* in the presence of ectopically expressed *cenR* was successful. Double crossover events were scored (phenotype: Spec<sup>R</sup>Kan<sup>S</sup>Suc<sup>R</sup>), and deletions confirmed by PCR (genotype). **(D)** Plasmid map of pIND5<sub>spec</sub>-*cenR* showing the location of primers used to confirm the presence of the plasmid by colony PCR. **(E)** Genomic positions and distances for the primers used in colony PCR to confirm the deletion of *cenR* (WT = 1,837 bp;  $\Delta$ *cenR* = 1,150 bp). (PDF)

**S3 Fig. Analysis of genome-wide transposon insertions within the *cenR* and *cenK* loci.**

Transposon insertion data determined previously by Burger *et. al.* (2017) [33]. The *Rb. sphaeroides* Tn5 mutant library was grown aerobically in Siström's minimal medium and split into two replicates (aliquots 1 and 2). Insertion positions and read count data for each genomic region are shown. **(A)** The genomic regions surrounding the nonessential gene *cenK* (*RSP\_1056*). **(B)** The genomic region surrounding the essential gene *cenR* (*RSP\_0847*). (PDF)

**S4 Fig. CenR(D56E) hyperactivity and cell elongation is independent of CenK activity.**

Bright-field microscopy measurements of the length of exponential phase cells displayed as beeswarm plots [135]. Mean values from each of the three biological replicates (grey circles, yellow triangles, and blue squares, respectively) and the mean value of cell length for each strain is shown (black bar). For each replicate  $n > 1000$  cells were analyzed. Unpaired t-tests were used to compare pooled cell dimension data from the mean values of each biological replicate ( $n = 3$ , \*  $P$  value  $< 0.05$ ). (Mean  $\pm$  SD) Wild-type:  $2.09 \pm 0.13 \mu\text{m}$ ; *cenR*(D56E)  $\Delta$ *cenK*:  $2.91 \pm 0.05 \mu\text{m}$ . (PDF)

**S5 Fig. CenR binds the promoters of *tolQRAB* and *rpoHI* in vitro.** Gel mobility shift assays containing DNA sequences directly upstream of *tolQ* (lanes 1–5), *rpoHI* (lanes 6–10), or *RSP\_2157* (lanes 11–15) transcription start sites [41]. To each reaction, 0, 125, 250, 500, or 1000 nM of phosphorylated CenR (CenR~P) was used to shift DNA. (PDF)

**S6 Fig. Putative CenR binding and regulation of the division and cell wall gene cluster.**

Shown are the ChIP-seq data traces of CenR binding upstream of an indicated promoter in TCS “on” strains (*cenR*(D56E) in green, and WT in black) and TCS “low activity” strains ( $\Delta$ *cenK* in red, and *cenR*(D56A) in orange). ChIP-seq peak heights are represented on the y-axis (fold-enrichment of IP vs input DNA). The chromosomal location is shown on the x-axis with genes represented by arrows pointing in the direction of transcription. TSSs of known promoter(s) are represented as green arrows [41,124]. This inset shows the log<sub>2</sub> fold change in transcript levels determined from RNA-seq experiments showing change in abundance of the

indicated gene in TCS mutant strains relative to WT cells. Non-significant (N.S.) changes in gene expression ( $FDR > 0.05$ ) are indicated with a grey box. **(A)** The first half of the *dcw* operon showing putative CenR enrichment within of the promoter region of *mraZ*. **(B)** The second half of the *dcw* operon showing CenR enrichment within the promoter regions of *ftsW* / *RSP\_2105* and *ddlA*. CenKR TCS activity is predicted to repress the transcription of genes in the *dcw* operon.

(PDF)

**S1 Table. The expanded CenKR regulon.**

(PDF)

**S2 Table. Primers, plasmids, and strains used in this study.**

(PDF)

**S3 Table. Genbank accession numbers for protein sequences used to construct CenK/R phylogeny.**

(PDF)

**S4 Table. PatSer motif search scores and the probability weight matrix (PWM) of the identified CenR binding motif.**

(PDF)

**S1 Data. MOSAiCS ChIP-seq peak dataset.**

(XLSX)

**S2 Data. RNA-seq dataset.**

(XLSX)

**S3 Data. Raw cell length and width measurements.**

(XLSX)

## Acknowledgments

We thank Kemardo K. Henry and the Gourse Lab (University of Wisconsin–Madison) for help setting up the phosphotransfer assays. Specific thank you to Sarah E. Moskal (UW–Madison), Rachelle A. Lemke (UW–Madison), Wayne S. Kontur (UW–Madison), Kimberly C. Lemmer (UW–Madison), and Katherine J. Wozniak (University of Michigan), as well as other members of the Donohue/ Noguera group for helpful discussion and feedback.

## Author Contributions

**Conceptualization:** Bryan D. Lakey, Erin L. Mettert, Patricia J. Kiley.

**Data curation:** Bryan D. Lakey, Kevin S. Myers.

**Formal analysis:** Bryan D. Lakey, Kevin S. Myers, François Alberge, Erin L. Mettert.

**Funding acquisition:** Daniel R. Noguera, Timothy J. Donohue.

**Investigation:** Bryan D. Lakey.

**Methodology:** Bryan D. Lakey, Erin L. Mettert, Patricia J. Kiley.

**Project administration:** Bryan D. Lakey.

**Resources:** Bryan D. Lakey.

**Supervision:** Daniel R. Noguera, Timothy J. Donohue.

**Validation:** Bryan D. Lakey.

**Visualization:** Bryan D. Lakey.

**Writing – original draft:** Bryan D. Lakey.

**Writing – review & editing:** Bryan D. Lakey, Patricia J. Kiley, Daniel R. Noguera, Timothy J. Donohue.

## References

1. Silhavy TJ, Kahne D, Walker S. The Bacterial Cell Envelope. *Cold Spring Harb Perspect Biol.* 2010; 2: a000414. <https://doi.org/10.1101/cshperspect.a000414> PMID: 20452953
2. Whitfield C, Trent MS. Biosynthesis and Export of Bacterial Lipopolysaccharides. *Annual Review of Biochemistry.* 2014; 83: 99–128. <https://doi.org/10.1146/annurev-biochem-060713-035600> PMID: 24580642
3. Rojas ER, Billings G, Odermatt PD, Auer GK, Zhu L, Miguel A, et al. The outer membrane is an essential load-bearing element in Gram-negative bacteria. *Nature.* 2018; 559: 617–621. <https://doi.org/10.1038/s41586-018-0344-3> PMID: 30022160
4. Vollmer W, Seligman SJ. Architecture of peptidoglycan: more data and more models. *Trends in Microbiology.* 2010; 18: 59–66. <https://doi.org/10.1016/j.tim.2009.12.004> PMID: 20060721
5. Egan AJF, Errington J, Vollmer W. Regulation of peptidoglycan synthesis and remodelling. *Nat Rev Microbiol.* 2020; 18: 446–460. <https://doi.org/10.1038/s41579-020-0366-3> PMID: 32424210
6. Stock AM, Robinson VL, Goudreau PN. Two-Component Signal Transduction. *Annual Review of Biochemistry.* 2000; 69: 183–215. <https://doi.org/10.1146/annurev.biochem.69.1.183> PMID: 10966457
7. Jacob-Dubuisson F, Mechaly A, Betton J-M, Antoine R. Structural insights into the signalling mechanisms of two-component systems. *Nat Rev Microbiol.* 2018; 16: 585–593. <https://doi.org/10.1038/s41579-018-0055-7> PMID: 30008469
8. Zschiedrich CP, Keidel V, Szurmant H. Molecular Mechanisms of Two-Component Signal Transduction. *Journal of Molecular Biology.* 2016; 428: 3752–3775. <https://doi.org/10.1016/j.jmb.2016.08.003> PMID: 27519796
9. Gao R, Stock AM. Biological Insights from Structures of Two-Component Proteins. *Annual Review of Microbiology.* 2009; 63: 133–154. <https://doi.org/10.1146/annurev.micro.091208.073214> PMID: 19575571
10. Raivio TL, Silhavy TJ. Transduction of envelope stress in *Escherichia coli* by the Cpx two-component system. *Journal of Bacteriology.* 1997; 179: 7724–7733. <https://doi.org/10.1128/jb.179.24.7724-7733.1997> PMID: 9401031
11. Grabowicz M, Silhavy TJ. Envelope Stress Responses: An Interconnected Safety Net. *Trends in Biochemical Sciences.* 2017; 42: 232–242. <https://doi.org/10.1016/j.tibs.2016.10.002> PMID: 27839654
12. May KL, Lehman KM, Mitchell AM, Grabowicz M. A Stress Response Monitoring Lipoprotein Trafficking to the Outer Membrane. *mBio.* 2019; 10: e00618–19. <https://doi.org/10.1128/mBio.00618-19> PMID: 31138744
13. Wall E, Majdalani N, Gottesman S. The Complex Rcs Regulatory Cascade. *Annual Review of Microbiology.* 2018; 72: 111–139. <https://doi.org/10.1146/annurev-micro-090817-062640> PMID: 29897834
14. Raffa RG, Raivio TL. A third envelope stress signal transduction pathway in *Escherichia coli*. *Molecular Microbiology.* 2002; 45: 1599–1611. <https://doi.org/10.1046/j.1365-2958.2002.03112.x> PMID: 12354228
15. Stein BJ, Fiebig A, Crosson S. The ChvG-Chvl and NtrY-NtrX Two-Component Systems Coordinately Regulate Growth of *Caulobacter crescentus*. *Journal of Bacteriology.* 2021; 203: e00199–21. <https://doi.org/10.1128/JB.00199-21> PMID: 34124942
16. Price NL, Raivio TL. Characterization of the Cpx regulon in *Escherichia coli* strain MC4100. *J Bacteriol.* 2009; 191: 1798–1815. <https://doi.org/10.1128/JB.00798-08> PMID: 19103922
17. Guest RL, Rutherford ST, Silhavy TJ. Border Control: Regulating LPS Biogenesis. *Trends in Microbiology.* 2021; 29: 334–345. <https://doi.org/10.1016/j.tim.2020.09.008> PMID: 33036869
18. García-Calderón CB, Casadesús J, Ramos-Morales F. Rcs and PhoPQ regulatory overlap in the control of *Salmonella enterica* virulence. *J Bacteriol.* 2007; 189: 6635–6644. <https://doi.org/10.1128/JB.00640-07> PMID: 17616593

19. Callewaert L, Vanoirbeek KGA, Lurquin I, Michiels CW, Aertsen A. The Rcs Two-Component System Regulates Expression of Lysozyme Inhibitors and Is Induced by Exposure to Lysozyme. *Journal of Bacteriology*. 2009; 191: 1979–1981. <https://doi.org/10.1128/JB.01549-08> PMID: 19136591
20. Bernal-Cabas M, Ayala JA, Raivio TL. The Cpx Envelope Stress Response Modifies Peptidoglycan Cross-Linking via the I,d-Transpeptidase LdtD and the Novel Protein YgaU. *Journal of Bacteriology*. 2015; 197: 603–614. <https://doi.org/10.1128/JB.02449-14> PMID: 25422305
21. Laubacher ME, Ades SE. The Rcs Phosphorelay Is a Cell Envelope Stress Response Activated by Peptidoglycan Stress and Contributes to Intrinsic Antibiotic Resistance. *Journal of Bacteriology*. 2008; 190: 2065–2074. <https://doi.org/10.1128/JB.01740-07> PMID: 18192383
22. Dörr T, Alvarez L, Delgado F, Davis BM, Cava F, Waldor MK. A cell wall damage response mediated by a sensor kinase/response regulator pair enables beta-lactam tolerance. *Proc Natl Acad Sci U S A*. 2016; 113: 404–409. <https://doi.org/10.1073/pnas.1520333113>
23. Gorla P, Plocinska R, Sarva K, Satsangi AT, Pandeeti E, Donnelly R, et al. MtrA Response Regulator Controls Cell Division and Cell Wall Metabolism and Affects Susceptibility of Mycobacteria to the First Line Antituberculosis Drugs. *Front Microbiol*. 2018; 9: 2839. <https://doi.org/10.3389/fmicb.2018.02839> PMID: 30532747
24. Zahrt TC, Deretic V. An Essential Two-Component Signal Transduction System in *Mycobacterium tuberculosis*. *Journal of Bacteriology*. 2000; 182: 3832–3838. <https://doi.org/10.1128/JB.182.13.3832-3838.2000> PMID: 10851001
25. Lemmer KC, Zhang W, Langer SJ, Dohnalkova AC, Hu D, Lemke RA, et al. Mutations That Alter the Bacterial Cell Envelope Increase Lipid Production. *mBio*. 2017; 8: e00513–17. <https://doi.org/10.1128/mBio.00513-17> PMID: 28536286
26. Skerker JM, Prasol MS, Perchuk BS, Biondi EG, Laub MT. Two-Component Signal Transduction Pathways Regulating Growth and Cell Cycle Progression in a Bacterium: A System-Level Analysis. *PLOS Biology*. 2005; 3: e334. <https://doi.org/10.1371/journal.pbio.0030334> PMID: 16176121
27. Burger L, Erik van N. Accurate prediction of protein–protein interactions from sequence alignments using a Bayesian method. *Molecular Systems Biology*. 2008; 4: 165. <https://doi.org/10.1038/msb4100203> PMID: 18277381
28. Shoemaker BA, Panchenko AR. Deciphering Protein–Protein Interactions. Part II. Computational Methods to Predict Protein and Domain Interaction Partners. *PLOS Computational Biology*. 2007; 3: e43. <https://doi.org/10.1371/journal.pcbi.0030043> PMID: 17465672
29. Capra EJ, Laub MT. Evolution of Two-Component Signal Transduction Systems. *Annual Review of Microbiology*. 2012; 66: 325–347. <https://doi.org/10.1146/annurev-micro-092611-150039> PMID: 22746333
30. Igo MM, Ninfa AJ, Stock JB, Silhavy TJ. Phosphorylation and dephosphorylation of a bacterial transcriptional activator by a transmembrane receptor. *Genes Dev*. 1989; 3: 1725–1734. <https://doi.org/10.1101/gad.3.11.1725> PMID: 2558046
31. Fisher SL, Kim S-K, Wanner BL, Walsh CT. Kinetic Comparison of the Specificity of the Vancomycin Resistance Kinase VanS for Two Response Regulators, VanR and PhoB. *Biochemistry*. 1996; 35: 4732–4740. <https://doi.org/10.1021/bi9525435> PMID: 8664263
32. Comolli JC, Carl AJ, Hall C, Donohue T. Transcriptional Activation of the *Rhodobacter sphaeroides* Cytochrome c2 Gene P2 Promoter by the Response Regulator PrrA. *J Bacteriol*. 2002; 184: 390–399. <https://doi.org/10.1128/JB.184.2.390-399.2002> PMID: 11751815
33. Burger BT, Imam S, Scarborough MJ, Noguera DR, Donohue TJ. Combining Genome-Scale Experimental and Computational Methods To Identify Essential Genes in *Rhodobacter sphaeroides*. *mSystems*. 2017; 2: e00015–17. <https://doi.org/10.1128/mSystems.00015-17> PMID: 28744485
34. Yang J, Yan R, Roy A, Xu D, Poisson J, Zhang Y. The I-TASSER Suite: protein structure and function prediction. *Nat Methods*. 2015; 12: 7–8. <https://doi.org/10.1038/nmeth.3213> PMID: 25549265
35. Roy A, Kucukural A, Zhang Y. I-TASSER: a unified platform for automated protein structure and function prediction. *Nat Protoc*. 2010; 5: 725–738. <https://doi.org/10.1038/nprot.2010.5> PMID: 20360767
36. Zhang Y. I-TASSER server for protein 3D structure prediction. *BMC Bioinformatics*. 2008; 9: 40. <https://doi.org/10.1186/1471-2105-9-40> PMID: 18215316
37. Zhao Z, Peng T, Oh J-I, Glaeser J, Weber L, Li Q, et al. A response regulator of the OmpR family is part of the regulatory network controlling the oxidative stress response of *Rhodobacter sphaeroides*. *Environmental Microbiology Reports*. 2019; 11: 118–128. <https://doi.org/10.1111/1758-2229.12718> PMID: 30451391
38. Smith JG, Latiolais JA, Guanga GP, Pennington JD, Silversmith RE, Bourret RB. A search for amino acid substitutions that universally activate response regulators. *Molecular Microbiology*. 2004; 51: 887–901. <https://doi.org/10.1046/j.1365-2958.2003.03882.x> PMID: 14731287

39. Klose KE, Weiss DS, Kustu S. Glutamate at the Site of Phosphorylation of Nitrogen-regulatory Protein NTRC Mimics Aspartyl-Phosphate and Activates the Protein. *Journal of Molecular Biology*. 1993; 232: 67–78. <https://doi.org/10.1006/jmbi.1993.1370> PMID: 8331671
40. Kuan PF, Chung D, Pan G, Thomson JA, Stewart R, Keleş S. A Statistical Framework for the Analysis of ChIP-Seq Data. *J Am Stat Assoc*. 2011; 106: 891–903. <https://doi.org/10.1198/jasa.2011.ap09706> PMID: 26478641
41. Myers KS, Vera JM, Lemmer KC, Linz AM, Landick R, Noguera DR, et al. Genome-Wide Identification of Transcription Start Sites in Two Alphaproteobacteria, *Rhodobacter sphaeroides* 2.4.1 and *Novosphingobium aromaticivorans* DSM 12444. *Microbiology Resource Announcements*. 2020; 9: e00880–20. <https://doi.org/10.1128/MRA.00880-20> PMID: 32883797
42. Bailey TL, Boden M, Buske FA, Frith M, Grant CE, Clementi L, et al. MEME Suite: tools for motif discovery and searching. *Nucleic Acids Research*. 2009; 37: W202–W208. <https://doi.org/10.1093/nar/gkp335> PMID: 19458158
43. Bailey TL, Williams N, Misleh C, Li WW. MEME: discovering and analyzing DNA and protein sequence motifs. *Nucleic Acids Research*. 2006; 34: W369–W373. <https://doi.org/10.1093/nar/gkl198> PMID: 16845028
44. Wang JC. Helical repeat of DNA in solution. *Proc Natl Acad Sci U S A*. 1979; 76: 200–203. <https://doi.org/10.1073/pnas.76.1.200> PMID: 284332
45. Krogh A, Larsson B, von Heijne G, Sonnhammer ELL. Predicting transmembrane protein topology with a hidden markov model: application to complete genomes<sup>1</sup> Edited by F. Cohen. *Journal of Molecular Biology*. 2001; 305: 567–580. <https://doi.org/10.1006/jmbi.2000.4315> PMID: 11152613
46. Almagro Armenteros JJ, Tsirigos KD, Sønderby CK, Petersen TN, Winther O, Brunak S, et al. SignalP 5.0 improves signal peptide predictions using deep neural networks. *Nat Biotechnol*. 2019; 37: 420–423. <https://doi.org/10.1038/s41587-019-0036-z> PMID: 30778233
47. Jeon Y, Lee YS, Han JS, Kim JB, Hwang DS. Multimerization of Phosphorylated and Non-phosphorylated ArcA Is Necessary for the Response Regulator Function of the Arc Two-component Signal Transduction System. *Journal of Biological Chemistry*. 2001; 276: 40873–40879. <https://doi.org/10.1074/jbc.M104855200> PMID: 11527965
48. Park DM, Akhtar MS, Ansari AZ, Landick R, Kiley PJ. The Bacterial Response Regulator ArcA Uses a Diverse Binding Site Architecture to Regulate Carbon Oxidation Globally. *PLOS Genetics*. 2013; 9: e1003839. <https://doi.org/10.1371/journal.pgen.1003839> PMID: 24146625
49. Jacoby GA. AmpC beta-lactamases. *Clin Microbiol Rev*. 2009; 22: 161–182, Table of Contents. <https://doi.org/10.1128/CMR.00036-08> PMID: 19136439
50. Mueller EA, Levin PA. Bacterial Cell Wall Quality Control during Environmental Stress. *mBio*. 2020; 11: e02456–20. <https://doi.org/10.1128/mBio.02456-20> PMID: 33051371
51. Aliashkevich A, Cava F. LD-transpeptidases: the great unknown among the peptidoglycan cross-linkers. *The FEBS Journal*. 2021. <https://doi.org/10.1111/febs.16066> PMID: 34109739
52. Malinverni JC, Silhavy TJ. An ABC transport system that maintains lipid asymmetry in the Gram-negative outer membrane. *Proceedings of the National Academy of Sciences*. 2009; 106: 8009–8014. <https://doi.org/10.1073/pnas.0903229106> PMID: 19383799
53. Sklar JG, Wu T, Kahne D, Silhavy TJ. Defining the roles of the periplasmic chaperones SurA, Skp, and DegP in *Escherichia coli*. *Genes Dev*. 2007; 21: 2473–2484. <https://doi.org/10.1101/gad.1581007> PMID: 17908933
54. Dufour YS, Imam S, Koo B-M, Green HA, Donohue TJ. Convergence of the Transcriptional Responses to Heat Shock and Singlet Oxygen Stresses. *PLOS Genetics*. 2012; 8: e1002929. <https://doi.org/10.1371/journal.pgen.1002929> PMID: 23028346
55. Depuydt M, Leonard SE, Vertommen D, Denoncin K, Morsomme P, Wahni K, et al. A Periplasmic Reducing System Protects Single Cysteine Residues from Oxidation. *Science*. 2009; 326: 1109–1111. <https://doi.org/10.1126/science.1179557> PMID: 19965429
56. Grimaud R, Ezraty B, Mitchell JK, Lafitte D, Briand C, Derrick PJ, et al. Repair of Oxidized Proteins: IDENTIFICATION OF A NEW METHIONINE SULFOXIDE REDUCTASE \*. *Journal of Biological Chemistry*. 2001; 276: 48915–48920. <https://doi.org/10.1074/jbc.M105509200> PMID: 11677230
57. Typas A, Banzhaf M, Gross CA, Vollmer W. From the regulation of peptidoglycan synthesis to bacterial growth and morphology. *Nat Rev Microbiol*. 2012; 10: 123–136. <https://doi.org/10.1038/nrmicro2677> PMID: 22203377
58. Hara H, Yasuda S, Horiuchi K, Park JT. A promoter for the first nine genes of the *Escherichia coli* mra cluster of cell division and cell envelope biosynthesis genes, including *ftsI* and *ftsW*. *Journal of Bacteriology*. 1997; 179: 5802–5811. <https://doi.org/10.1128/jb.179.18.5802-5811.1997> PMID: 9294438

59. Williams KP, Sobral BW, Dickerman AW. A Robust Species Tree for the Alphaproteobacteria. *Journal of Bacteriology*. 2007; 189: 4578–4586. <https://doi.org/10.1128/JB.00269-07> PMID: 17483224
60. Hördt A, López MG, Meier-Kolthoff JP, Schleuning M, Weinhold L-M, Tindall BJ, et al. Analysis of 1,000+ Type-Strain Genomes Substantially Improves Taxonomic Classification of Alphaproteobacteria. *Frontiers in Microbiology*. 2020; 11: 468. <https://doi.org/10.3389/fmicb.2020.00468> PMID: 32373076
61. Ferla MP, Thrash JC, Giovannoni SJ, Patrick WM. New rRNA Gene-Based Phylogenies of the Alpha-proteobacteria Provide Perspective on Major Groups, Mitochondrial Ancestry and Phylogenetic Instability. *PLOS ONE*. 2013; 8: e83383. <https://doi.org/10.1371/journal.pone.0083383> PMID: 24349502
62. Muñoz-Gómez SA, Hess S, Burger G, Lang BF, Susko E, Slamovits CH, et al. An updated phylogeny of the Alphaproteobacteria reveals that the parasitic Rickettsiales and Holosporales have independent origins. Rokas A, Wittkopp PJ, Irisarri I, editors. *eLife*. 2019; 8: e42535. <https://doi.org/10.7554/eLife.42535> PMID: 30789345
63. Pechter KB, Gallagher L, Pyles H, Manoil CS, Harwood CS. Essential Genome of the Metabolically Versatile Alphaproteobacterium *Rhodospseudomonas palustris*. *J Bacteriol*. 2015; 198: 867–876. <https://doi.org/10.1128/JB.00771-15> PMID: 26712940
64. Lemmer KC, Alberge F, Myers KS, Dohnalkova AC, Schaub RE, Lenz JD, et al. The NtrYX Two-Component System Regulates the Bacterial Cell Envelope. Harwood CS, editor. *mBio*. 2020; 11. <https://doi.org/10.1128/mBio.00957-20> PMID: 32430476
65. Dilani Senadheera M., Bernard Guggenheim, Spatafora Grace A., Cathy Huang Yi-Chen, Jison Choi, Hung David C. I., et al. A VicRK Signal Transduction System in *Streptococcus mutans* Affects *gtfBCD*, *gbpB*, and *fff* Expression, Biofilm Formation, and Genetic Competence Development. *Journal of Bacteriology*. 2005; 187: 4064–4076. <https://doi.org/10.1128/JB.187.12.4064-4076.2005> PMID: 15937169
66. Bisicchia P, Noone D, Lioliou E, Howell A, Quigley S, Jensen T, et al. The essential YycFG two-component system controls cell wall metabolism in *Bacillus subtilis*. *Mol Microbiol*. 2007; 65: 180–200. <https://doi.org/10.1111/j.1365-2958.2007.05782.x> PMID: 17581128
67. Saha S, Lach SR, Konovalova A. Homeostasis of the Gram-negative cell envelope. *Current Opinion in Microbiology*. 2021; 61: 99–106. <https://doi.org/10.1016/j.mib.2021.03.008> PMID: 33901778
68. Typas A, Banzhaf M, van den Berg van Saparoea B, Verheul J, Biboy J, Nichols RJ, et al. Regulation of peptidoglycan synthesis by outer membrane proteins. *Cell*. 2010; 143: 1097–1109. <https://doi.org/10.1016/j.cell.2010.11.038> PMID: 21183073
69. Gerding MA, Ogata Y, Pecora ND, Niki H, De Boer PAJ. The trans-envelope Tol–Pal complex is part of the cell division machinery and required for proper outer-membrane invagination during cell constriction in *E. coli*. *Molecular Microbiology*. 2007; 63: 1008–1025. <https://doi.org/10.1111/j.1365-2958.2006.05571.x> PMID: 17233825
70. Szczepaniak J, Holmes P, Rajasekar K, Kaminska R, Samsudin F, Inns PG, et al. The lipoprotein Pal stabilises the bacterial outer membrane during constriction by a mobilisation-and-capture mechanism. *Nat Commun*. 2020; 11: 1305. <https://doi.org/10.1038/s41467-020-15083-5> PMID: 32161270
71. Yakhnina AA, Bernhardt TG. The Tol-Pal system is required for peptidoglycan-cleaving enzymes to complete bacterial cell division. *Proc Natl Acad Sci USA*. 2020; 117: 6777–6783. <https://doi.org/10.1073/pnas.1919267117> PMID: 32152098
72. Gray AN, Egan AJ, van't Veer IL, Verheul J, Colavin A, Koumoutsis A, et al. Coordination of peptidoglycan synthesis and outer membrane constriction during *Escherichia coli* cell division. Storz G, editor. *eLife*. 2015; 4: e07118. <https://doi.org/10.7554/eLife.07118> PMID: 25951518
73. Yeh Y-C, Comolli LR, Downing KH, Shapiro L, McAdams HH. The Caulobacter Tol-Pal Complex Is Essential for Outer Membrane Integrity and the Positioning of a Polar Localization Factor. *Journal of Bacteriology*. 2010; 192: 4847–4858. <https://doi.org/10.1128/JB.00607-10> PMID: 20693330
74. Godessart P, Lannoy A, Dieu M, Van der Verren SE, Soumillion P, Collet J-F, et al.  $\beta$ -Barrels covalently link peptidoglycan and the outer membrane in the  $\alpha$ -proteobacterium *Brucella abortus*. *Nat Microbiol*. 2021; 6: 27–33. <https://doi.org/10.1038/s41564-020-00799-3> PMID: 33139884
75. Szczepaniak J, Press C, Kleantous C. The multifarious roles of Tol-Pal in Gram-negative bacteria. *FEMS Microbiol Rev*. 2020; 44: 490–506. <https://doi.org/10.1093/femsre/fuaa018> PMID: 32472934
76. Shrivastava R, Jiang X, Chng S-S. Outer membrane lipid homeostasis via retrograde phospholipid transport in *Escherichia coli*. *Mol Microbiol*. 2017; 106: 395–408. <https://doi.org/10.1111/mmi.13772> PMID: 28815827
77. Krol E, Yau HCL, Lechner M, Schäper S, Bange G, Vollmer W, et al. Tol-Pal System and Rgs Proteins Interact to Promote Unipolar Growth and Cell Division in *Sinorhizobium meliloti*. *mBio*. 2020; 11: e00306–20. <https://doi.org/10.1128/mBio.00306-20> PMID: 32605980

78. Konovalova A, Grabowicz M, Balibar CJ, Malinverni JC, Painter RE, Riley D, et al. Inhibitor of intramembrane protease RseP blocks the  $\sigma^E$  response causing lethal accumulation of unfolded outer membrane proteins. *Proc Natl Acad Sci USA*. 2018; 115: E6614. <https://doi.org/10.1073/pnas.1806107115> PMID: 29941590
79. Vianney A, Muller MM, Clavel T, Lazzaroni JC, Portalier R, Webster RE. Characterization of the tol-pal region of *Escherichia coli* K-12: translational control of tolR expression by TolQ and identification of a new open reading frame downstream of pal encoding a periplasmic protein. *Journal of Bacteriology*. 1996; 178: 4031–4038. <https://doi.org/10.1128/jb.178.14.4031-4038.1996> PMID: 8763928
80. Clavel T, Lazzaroni JC, Vianney A, Portalier R. Expression of the tolQRA genes of *Escherichia coli* K-12 is controlled by the RcsC sensor protein involved in capsule synthesis. *Mol Microbiol*. 1996; 19: 19–25. <https://doi.org/10.1046/j.1365-2958.1996.343880.x> PMID: 8821933
81. Green HA, Donohue TJ. Activity of *Rhodobacter sphaeroides* RpoHII, a Second Member of the Heat Shock Sigma Factor Family. *J Bacteriol*. 2006; 188: 5712–5721. <https://doi.org/10.1128/JB.00405-06> PMID: 16885439
82. Nuss AM, Adnan F, Weber L, Berghoff BA, Glaeser J, Klug G. DegS and RseP Homologous Proteases Are Involved in Singlet Oxygen Dependent Activation of RpoE in *Rhodobacter sphaeroides*. *PLOS ONE*. 2013; 8: e79520. <https://doi.org/10.1371/journal.pone.0079520> PMID: 24223961
83. Csonka LN. Physiological and genetic responses of bacteria to osmotic stress. 1989; 53: 121–147. <https://doi.org/10.1128/mr.53.1.121-147.1989> PMID: 2651863
84. Daitch AK, Orsburn BC, Chen Z, Alvarez L, Eberhard CD, Sundararajan K, et al. EstG is a novel esterase required for cell envelope integrity. *BioRxiv [PrePrint]*. 2022. <https://doi.org/10.1101/2022.04.12.488081>
85. Kiley PJ, Kaplan S. Molecular genetics of photosynthetic membrane biosynthesis in *Rhodobacter sphaeroides*. 1988; 52: 50–69. <https://doi.org/10.1128/mr.52.1.50-69.1988>
86. LaSarre B, Kysela DT, Stein BD, Ducret A, Brun YV, McKinlay JB. Restricted Localization of Photosynthetic Intracytoplasmic Membranes (ICMs) in Multiple Genera of Purple Nonsulfur Bacteria. *mBio*. 2018; 9: e00780–18. <https://doi.org/10.1128/mBio.00780-18> PMID: 29970460
87. Ryan KR, Shapiro L. Temporal and Spatial Regulation in Prokaryotic Cell Cycle Progression and Development. *Annu Rev Biochem*. 2003; 72: 367–394. <https://doi.org/10.1146/annurev.biochem.72.121801.161824> PMID: 12651741
88. Brown PJB, de Pedro MA, Kysela DT, Van der Henst C, Kim J, De Bolle X, et al. Polar growth in the Alphaproteobacterial order Rhizobiales. *Proc Natl Acad Sci U S A*. 2012; 109: 1697–1701. <https://doi.org/10.1073/pnas.1114476109> PMID: 22307633
89. Watarai M, Makino S, Fujii Y, Okamoto K, Shirahata T. Modulation of Brucella-induced macropinocytosis by lipid rafts mediates intracellular replication. *Cellular Microbiology*. 2002; 4: 341–355. <https://doi.org/10.1046/j.1462-5822.2002.00195.x> PMID: 12067319
90. Howell M, Aliashkevich A, Sundararajan K, Daniel JJ, Lariviere PJ, Goley ED, et al. *Agrobacterium tumefaciens* divisome proteins regulate the transition from polar growth to cell division. *Molecular Microbiology*. 2019; 111: 1074–1092. <https://doi.org/10.1111/mmi.14212> PMID: 30693575
91. Sohlenkamp C, Geiger O. Bacterial membrane lipids: diversity in structures and pathways. *FEMS Microbiology Reviews*. 2016; 40: 133–159. <https://doi.org/10.1093/femsre/fuv008> PMID: 25862689
92. Otten C, Brill M, Vollmer W, Viollier PH, Salje J. Peptidoglycan in obligate intracellular bacteria. *Mol Microbiol*. 2018; 107: 142–163. <https://doi.org/10.1111/mmi.13880> PMID: 29178391
93. Atwal S, Chuenklin S, Bonder EM, Flores J, Gillespie JJ, Driscoll TP, et al. Discovery of a Diverse Set of Bacteria That Build Their Cell Walls without the Canonical Peptidoglycan Polymerase aPBP. *mBio*. 2021; 12: e0134221. <https://doi.org/10.1128/mBio.01342-21> PMID: 34311584
94. Pawlowski K, Klosse U, de Bruijn FJ. Characterization of a novel *Azorhizobium caulinodans* ORS571 two-component regulatory system, NtrY/NtrX, involved in nitrogen fixation and metabolism. *Molec Gen Genet*. 1991; 231: 124–138. <https://doi.org/10.1007/BF00293830> PMID: 1661370
95. Calatrava-Morales N, Nogales J, Amezttoy K, van Steenberg B, Soto MJ. The NtrY/NtrX System of *Sinorhizobium meliloti* GR4 Regulates Motility, EPS I Production, and Nitrogen Metabolism but Is Dispensable for Symbiotic Nitrogen Fixation. *MPMI*. 2017; 30: 566–577. <https://doi.org/10.1094/MPMI-01-17-0021-R> PMID: 28398840
96. López MF, Hegel VA, Torres MJ, García AH, Delgado MJ, López-García SL. The Bradyrhizobium diazoefficiens two-component fixation system NtrYX has a key role in symbiotic nitrogen fixation of soybean plants and cbb3 oxidase expression in bacteroids. *Plant Soil*. 2019; 440: 167–183. <https://doi.org/10.1007/s11104-019-04067-0>
97. Atack JM, Srikhanta YN, Djoko KY, Welch JP, Hasri NHM, Steichen CT, et al. Characterization of an ntrX Mutant of *Neisseria gonorrhoeae* Reveals a Response Regulator That Controls Expression of

- Respiratory Enzymes in Oxidase-Positive Proteobacteria. *Journal of Bacteriology*. 2013; 195: 2632–2641. <https://doi.org/10.1128/JB.02062-12> PMID: 23564168
98. Carrica M del C, Fernandez I, Martí MA, Paris G, Goldbaum FA. The NtrY/X two-component system of *Brucella* spp. acts as a redox sensor and regulates the expression of nitrogen respiration enzymes. *Molecular Microbiology*. 2012; 85: 39–50. <https://doi.org/10.1111/j.1365-2958.2012.08095.x> PMID: 22582926
  99. Wang D, Xue H, Wang Y, Yin R, Xie F, Luo L. The *Sinorhizobium meliloti* ntrX Gene Is Involved in Succinoglycan Production, Motility, and Symbiotic Nodulation on Alfalfa. *Applied and Environmental Microbiology*. 2013; 79: 7150–7159. <https://doi.org/10.1128/AEM.02225-13> PMID: 24038694
  100. Charles TC, Nester EW. A chromosomally encoded two-component sensory transduction system is required for virulence of *Agrobacterium tumefaciens*. *J Bacteriol*. 1993; 175: 6614–6625. <https://doi.org/10.1128/jb.175.20.6614-6625.1993> PMID: 8407839
  101. Sola-Landa A, Pizarro-Cerdá J, Grilló MJ, Moreno E, Moriyón I, Blasco JM, et al. A two-component regulatory system playing a critical role in plant pathogens and endosymbionts is present in *Brucella abortus* and controls cell invasion and virulence. *Mol Microbiol*. 1998; 29: 125–138. <https://doi.org/10.1046/j.1365-2958.1998.00913.x> PMID: 9701808
  102. Yao S-Y, Luo L, Har KJ, Becker A, Rüberg S, Yu G-Q, et al. *Sinorhizobium meliloti* ExoR and ExoS proteins regulate both succinoglycan and flagellum production. *J Bacteriol*. 2004; 186: 6042–6049. <https://doi.org/10.1128/JB.186.18.6042-6049.2004> PMID: 15342573
  103. Wu C-F, Lin J-S, Shaw G-C, Lai E-M. Acid-Induced Type VI Secretion System Is Regulated by ExoR-ChvG/ChvI Signaling Cascade in *Agrobacterium tumefaciens*. *PLOS Pathogens*. 2012; 8: e1002938. <https://doi.org/10.1371/journal.ppat.1002938> PMID: 23028331
  104. Siström WRY. A Requirement for Sodium in the Growth of *Rhodospseudomonas spheroides*. *Microbiology*. 1960; 22: 778–785. <https://doi.org/10.1099/00221287-22-3-778> PMID: 14447230
  105. Schäfer A, Tauch A, Jäger W, Kalinowski J, Thierbach G, Pühler A. Small mobilizable multi-purpose cloning vectors derived from the *Escherichia coli* plasmids pK18 and pK19: selection of defined deletions in the chromosome of *Corynebacterium glutamicum*. *Gene*. 1994; 145: 69–73. [https://doi.org/10.1016/0378-1119\(94\)90324-7](https://doi.org/10.1016/0378-1119(94)90324-7) PMID: 8045426
  106. Simon R, Priefer U, Puhler A. A Broad Host Range Mobilization System for In Vivo Genetic Engineering: Transposon Mutagenesis in Gram Negative Bacteria. *Bio/Technology*. 1983; 1: 784–791. <https://doi.org/10.1038/NBT1183-784>
  107. Schindelin J, Arganda-Carreras I, Frise E, Kaynig V, Longair M, Pietzsch T, et al. Fiji: an open-source platform for biological-image analysis. *Nat Methods*. 2012; 9: 676–682. <https://doi.org/10.1038/nmeth.2019> PMID: 22743772
  108. Ducret A, Quardokus EM, Brun YV. MicrobeJ, a tool for high throughput bacterial cell detection and quantitative analysis. *Nat Microbiol*. 2016; 1: 1–7. <https://doi.org/10.1038/nmicrobiol.2016.77> PMID: 27572972
  109. Wickham H. ggplot2: Elegant Graphics for Data Analysis. New York, NY: Springer; 2009. <https://doi.org/10.1007/978-0-387-98141-3>
  110. Gall DL, Ralph J, Donohue TJ, Noguera DR. A Group of Sequence-Related Sphingomonad Enzymes Catalyzes Cleavage of  $\beta$ -Aryl Ether Linkages in Lignin  $\beta$ -Guaiaacyl and  $\beta$ -Syringyl Ether Dimers. *Environ Sci Technol*. 2014; 48: 12454–12463. <https://doi.org/10.1021/es503886d> PMID: 25232892
  111. Doherty AJ, Ashford SR, Brannigan JA, Wigley DB. A superior host strain for the over-expression of cloned genes using the T7 promoter based vectors. *Nucleic Acids Res*. 1995; 23: 2074–2075. <https://doi.org/10.1093/nar/23.11.2074> PMID: 7596839
  112. Wood WB. Host specificity of DNA produced by *Escherichia coli*: bacterial mutations affecting the restriction and modification of DNA. *J Mol Biol*. 1966; 16: 118–133. [https://doi.org/10.1016/s0022-2836\(66\)80267-x](https://doi.org/10.1016/s0022-2836(66)80267-x) PMID: 5331240
  113. Bolger AM, Lohse M, Usadel B. Trimmomatic: a flexible trimmer for Illumina sequence data. *Bioinformatics*. 2014; 30: 2114–2120. <https://doi.org/10.1093/bioinformatics/btu170> PMID: 24695404
  114. Langmead B, Salzberg SL. Fast gapped-read alignment with Bowtie 2. *Nat Methods*. 2012; 9: 357–359. <https://doi.org/10.1038/nmeth.1923> PMID: 22388286
  115. Anders S, Pyl PT, Huber W. HTSeq—a Python framework to work with high-throughput sequencing data. *Bioinformatics*. 2015; 31: 166–169. <https://doi.org/10.1093/bioinformatics/btu638> PMID: 25260700
  116. Robinson MD, McCarthy DJ, Smyth GK. edgeR: a Bioconductor package for differential expression analysis of digital gene expression data. *Bioinformatics*. 2010; 26: 139–140. <https://doi.org/10.1093/bioinformatics/btp616> PMID: 19910308

117. McCarthy DJ, Chen Y, Smyth GK. Differential expression analysis of multifactor RNA-Seq experiments with respect to biological variation. *Nucleic Acids Research*. 2012; 40: 4288–4297. <https://doi.org/10.1093/nar/gks042> PMID: 22287627
118. Benjamini Y, Hochberg Y. Controlling the False Discovery Rate: A Practical and Powerful Approach to Multiple Testing. *Journal of the Royal Statistical Society: Series B (Methodological)*. 1995; 57: 289–300. <https://doi.org/10.1111/j.2517-6161.1995.tb02031.x>
119. Karp PD, Billington R, Caspi R, Fulcher CA, Latendresse M, Kothari A, et al. The BioCyc collection of microbial genomes and metabolic pathways. *Briefings in Bioinformatics*. 2019; 20: 1085–1093. <https://doi.org/10.1093/bib/bbx085> PMID: 29447345
120. Broad Institute. Picard Toolkit. <http://broadinstitute.github.io/picard/>. 2019.
121. Li H, Handsaker B, Wysoker A, Fennell T, Ruan J, Homer N, et al. The Sequence Alignment/Map format and SAMtools. *Bioinformatics*. 2009; 25: 2078–2079. <https://doi.org/10.1093/bioinformatics/btp352> PMID: 19505943
122. Sun G, Chung D, Liang K, Keleş S. Statistical Analysis of ChIP-seq Data with MOSAiCS. In: Shomron N, editor. *Deep Sequencing Data Analysis*. Totowa, NJ: Humana Press; 2013. p. 193–212. [https://doi.org/10.1007/978-1-62703-514-9\\_12](https://doi.org/10.1007/978-1-62703-514-9_12)
123. Althammer S, González-Vallinas J, Ballaré C, Beato M, Eyrales E. Pyicos: a versatile toolkit for the analysis of high-throughput sequencing data. *Bioinformatics*. 2011; 27: 3333–3340. <https://doi.org/10.1093/bioinformatics/btr570> PMID: 21994224
124. Valouev A, Johnson DS, Sundquist A, Medina C, Anton E, Batzoglou S, et al. Genome-wide analysis of transcription factor binding sites based on ChIP-Seq data. *Nat Methods*. 2008; 5: 829–834. <https://doi.org/10.1038/nmeth.1246> PMID: 19160518
125. Homann OR, Johnson AD. MochiView: versatile software for genome browsing and DNA motif analysis. *BMC Biology*. 2010; 8: 49. <https://doi.org/10.1186/1741-7007-8-49> PMID: 20409324
126. Myers KS, Noguera DR, Donohue TJ. Promoter Architecture Differences among Alphaproteobacteria and Other Bacterial Taxa. *mSystems*. 2021; 6: e00526–21. <https://doi.org/10.1128/mSystems.00526-21> PMID: 34254822
127. Altschul SF, Gish W, Miller W, Myers EW, Lipman DJ. Basic local alignment search tool. *J Mol Biol*. 1990; 215: 403–410. [https://doi.org/10.1016/S0022-2836\(05\)80360-2](https://doi.org/10.1016/S0022-2836(05)80360-2) PMID: 2231712
128. Camacho C, Coulouris G, Avagyan V, Ma N, Papadopoulos J, Bealer K, et al. BLAST+: architecture and applications. *BMC Bioinformatics*. 2009; 10: 421. <https://doi.org/10.1186/1471-2105-10-421> PMID: 20003500
129. Tamura K, Stecher G, Peterson D, Filipiński A, Kumar S. MEGA6: Molecular Evolutionary Genetics Analysis version 6.0. *Mol Biol Evol*. 2013; 30: 2725–2729. <https://doi.org/10.1093/molbev/mst197> PMID: 24132122
130. Edgar RC. MUSCLE: multiple sequence alignment with high accuracy and high throughput. *Nucleic Acids Research*. 2004; 32: 1792–1797. <https://doi.org/10.1093/nar/gkh340> PMID: 15034147
131. Talavera G, Castresana J. Improvement of Phylogenies after Removing Divergent and Ambiguously Aligned Blocks from Protein Sequence Alignments. *Systematic Biology*. 2007; 56: 564–577. <https://doi.org/10.1080/10635150701472164> PMID: 17654362
132. Price MN, Dehal PS, Arkin AP. FastTree 2 – Approximately Maximum-Likelihood Trees for Large Alignments. *PLOS ONE*. 2010; 5: e9490. <https://doi.org/10.1371/journal.pone.0009490> PMID: 20224823
133. Benítez-Bellón E, Moreno-Hagelsieb G, Collado-Vides J. Evaluation of thresholds for the detection of binding sites for regulatory proteins in *Escherichia coli* K12 DNA. *Genome Biol*. 2002; 3: RESEARCH0013. <https://doi.org/10.1186/gb-2002-3-3-research0013> PMID: 11897025
134. Crooks GE, Hon G, Chandonia J-M, Brenner SE. WebLogo: a sequence logo generator. *Genome Res*. 2004; 14: 1188–1190. <https://doi.org/10.1101/gr.849004> PMID: 15173120
135. Lord SJ, Velle KB, Mullins RD, Fritz-Laylin LK. SuperPlots: Communicating reproducibility and variability in cell biology. *Journal of Cell Biology*. 2020; 219. <https://doi.org/10.1083/jcb.202001064> PMID: 32346721